Available online at www.sciencedirect.com
SCIENCE DIRECT®
Chemie der Erde 65 (2005) 47–78
CHEMIE der ERDE GEOCHEMISTRY
www.elsevier.de/chemer

Geochemical and isotopic characteristics and evolution of the Jurassic volcanic arc between Arica (18°30′S) and Tocopilla (22°S), North Chilean Coastal Cordillera

Wolfgang Kramer[a,*], Wolfgang Siebel[a,1], Rolf L. Romer[a], Günther Haase[a], Martin Zimmer[a], Ralph Ehrlichmann[b]

[a] *GeoForschungsZentrum Potsdam, Telegrafenberg, 14473 Potsdam, Germany*
[b] *TU Berlin, Strasse des 17. Juni 135, 10623 Berlin, Germany*

Received 1 November 2003; accepted 5 January 2004

Abstract

The present-day North Chilean Coastal Cordillera between 18°30′S and 22°S records an important part of the magmatic evolution of the Central Andes during the Jurassic. Calc-alkaline to subordinate tholeiitic members from four rock groups with biostratigraphically constrained age display incompatible element pattern characteristic of convergent plate-margin volcanism, whereas alkaline basalts of one group occurring in the Precordillera show OIB-type trace element signatures. The correlation of biostratigraphic ages, regional distribution, and composition of the volcanic rocks provides a basis for the discussion on geochemical evolution and isotope ratios.

Major and trace element distributions of the volcanic rocks indicate their derivation from mantle-derived melts. LILE and LREE enrichments in calc-alkaline basaltic andesites to dacites and some of the tholeiites hint at the involvement of hydrous fluids during melting and mobile element transport processes. A part of the Early Bajocian to ?Lower Jurassic and Oxfordian andesites and dacites are adakite-like rocks with a substantial participation of slab melt and are characterized by high Sr/Y ratios and low HREE contents. The Middle Jurassic tholeiitic and calc-alkaline basalts and basaltic andesites have been transported and partly

*Corresponding author. Fax +49-0-331-288-1316.
E-mail addresses: kraw@gfz-potsdam.de (W. Kramer), wolfgang.siebel@uni-tuebingen.de (W. Siebel).
[1] Present address: Institut für Geowissenschaften, Universität Tübingen, Wilhelmstraße 56, 72074 Tübingen, Germany.

doi:10.1016/j.chemer.2004.01.002

stored within a system of deep-seated feeder fissures and crustal strike-slip faults before eruption.

The isotopic composition of Sr ($^{87}Sr/^{86}Sr_i = 0.7032–0.7056$) and Nd ($\varepsilon Nd_i = 2.2-7.1$) of the Jurassic volcanic rocks mostly fall in the range characteristic for mantle melts although some crustal components may have been involved. A few samples show slightly more radiogenic Sr isotopic composition, which is probably due to interaction with ancient sea-water. The Pb isotopic composition of the arc rocks is uncoupled from the isotopic composition of Sr and Nd and is dominated by the crustal component. Since the Cretaceous and Modern arc volcanic rocks show Pb isotopic compositions that can be largely explained by in situ Pb isotope growth of Jurassic arc volcanic rocks, we argue that the various Andean arc systems between 18°30′S and 22°S formed on the same type of basement.

Most of the investigated samples have high Ba, Zr, and Th concentrations compared to island arc mafic volcanic rocks. About 20% of the Jurassic arc volcanics comprise of dacitic to rhyolitic rocks. These characteristics combined with the Pb isotopic composition that shows the influence of a Palaeozoic (or partly older) basement point to a continental margin setting for the North Chilean Jurassic arc. The distribution of the magmatic rocks throughout time, their textures, and the character of intercalated sedimentary rocks reflect westward movement of the magma sources and of the arc/back-arc boundary relative to the current coast line during the Early Bajocian on a broad front between 19°30′ and 21°S.

Keywords: Trace elements; Sr; Nd and Pb isotopes; Basaltic andesite; Alkaline basalt; Adakite; Jurassic arc; Tectonic setting; Coastal Cordillera; N-Chile

1. Introduction

The Jurassic volcanic-sedimentary formations of the North-Chilean Coastal Cordillera between 18°30′S and 22°S (Fig. 1) belong to the former western margin of Gondwana, where according to Jaillard et al. (1990) and Sempére (1995) the subduction of Paleopacific (and later Phoenix) oceanic plates during the Upper Triassic/Lower Jurassic took place. This process controlled the evolution of the Early Andes (Coira et al., 1982; Mpodozis and Ramos, 1990).

The geological setting and magma sources during the early Andean Jurassic volcanic development of the North-Chilean Coastal Cordillera is discussed controversially. Earlier workers interpreted the Jurassic volcanic rocks either as part of a volcanic arc at an active continental margin (Davidson et al., 1976; Coira et al., 1982) or as part of an island arc (Palacios, 1978). According to Rogers and Hawkesworth (1989), volcanic rocks of the main Jurassic La Negra Formation were formed in an ensialic backarc-basin setting. Based on trace element data, Buchelt and Tellez (1988) likewise argued that the La Negra rocks were formed in a backarc setting and show chemical affinities to within plate basalts. Lucassen et al. (1996) explained the generation of the La Negra melts by decompressional melting in the lithospheric mantle, without the subduction processes being involved. Jurassic volcanism controlled by pull-apart type structures caused by oblique subduction (since 190 Ma) was proposed by Scheuber and Reutter (1992) and Pichowiak (1994).

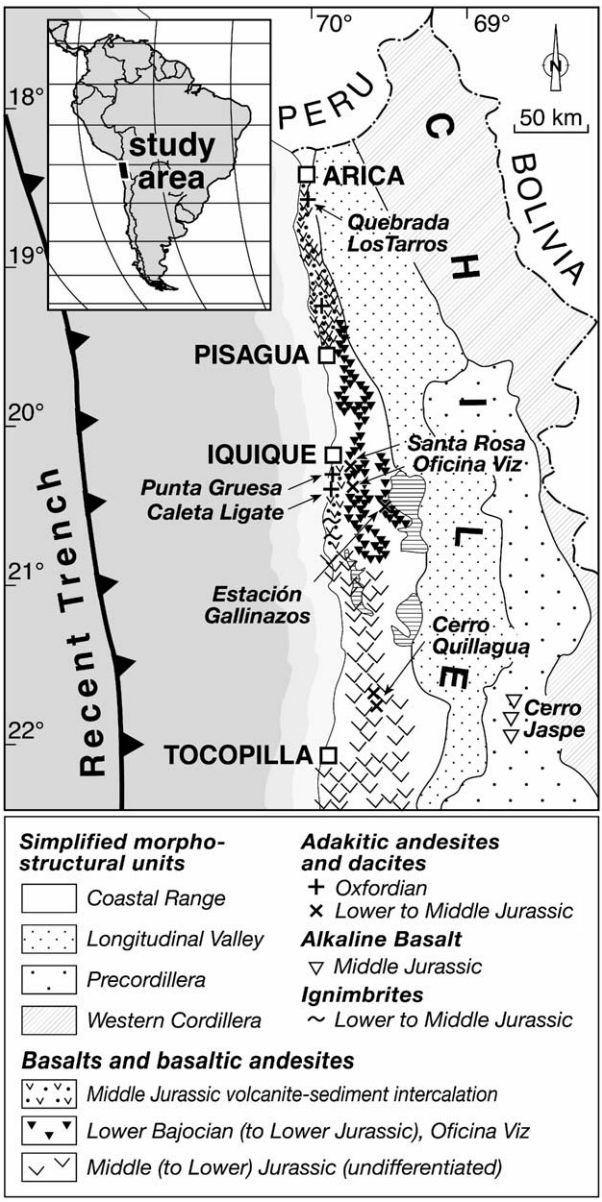

Fig. 1. Geological sketch map of the study area in the North Chilean Coastal Range between 18°30′ and 22°S. Note the shift of the Jurassic volcanic activities from east (Oficina Viz Fm.) on a wide front to the west (Caleta Ligate Fm.).

These contrasting interpretations are based, inter alia, on few samples and on limited data spectra from a restricted area around Antofagasta–Tocopilla. In the Antofagasta area, biostratigraphic ages are available only from the lowest part

(Sinemurian) of the volcanic series. In the northern arc section, the Iquique–Arica area, however, the age of the volcanic rocks is bracketed by intercalated fossil-bearing sedimentary rocks over a much longer period (Kossler, 1998; Wittmann, 1999). Therefore, we focus on volcanic rock profiles from the coastal range near Iquique and Arica. The volcanic rocks of the studied area mainly comprise basalts, basaltic andesites, dacites, and subordinate andesites and acid ignimbrites, which in part show compositional similarities to volcanic rocks of the La Negra Formation near Antofagasta (Buchelt and Zeil, 1986; von Hillebrandt et al., 1998). Element and isotope data presented in this study contribute to the genetical characterization of Jurassic volcanic activities in the northernmost Chilean arc section of about 250 km length, which is prominent by its position immediately south of the present-day Andean bend (Arica elbow; Fig. 1). The data allow to correlate the evolution of volcanism and tectonics in terms of oblique subduction resulting in changing strike-slip and extensional regimes. In addition, the data feature the volcanic series as important component of a continental margin setting.

2. Geologic background

2.1. Field relations and rock description

Within the Coastal Cordillera of the Central Andes, the Jurassic rocks are exposed in a northward narrowing wedge-like pattern (Fig. 1). A positive gravity anomaly (Kösters et al., 1997), however, indicates that considerable parts of the northern Jurassic arc extend offshore towards the present-day trench. Our study area comprises the northern part of the Chilean Jurassic arc. This section has been largely destroyed by post-Jurassic subduction erosion (von Huene et al., 1999; Pelz, 2000). Between 18°30′ and 21° south, the remnants of the Jurassic lava piles cover an area of 4000 km^2 on land. Mafic volcanic rocks of the ?Lower to Middle Jurassic Officina Viz Formation and Oxfordian lavas are still preserved within the interior coastal range southeast of Iquique and Arica, whereas the volcanic rocks of the Middle to Upper Jurassic Caleta Ligate and El Godo formation as well as volcanic rocks of the Punta Gruesa area occur at the present shore and offshore. The only known Jurassic lavas within the present-day Chilean Precordillera at these latitudes extruded in the Cerro Jaspe area to the north of Chuquicamata (Fig. 1).

Detailed lithologic, paleogeographic, and biostratigraphic work demonstrates that the arc and the arc–backarc boundary in the Iquique area moved to the west during the Early Bajocian (Kossler, 1998; von Hillebrandt et al., 2000). The Lower to Middle Jurassic volcanic complexes are made up of thick extensive lava piles in the interior Coastal Cordillera and pillow piles with intercalated lava flows along the coast and offshore. Apparently, these lavas were fed from fissures or small vents that were controlled by transtensional pull-apart or extensional structures as described by Scheuber and Reutter (1992), Grocott et al. (1994), Pichowiak (1994) and Scheuber and Gonzalez (1999). These tectonic structures might have resulted from oblique

Table 1. Investigated samples and their stage, formation, and biostratigraphic age using the Mesozoic time scale from Pálfy et al. (2000)

Stage	Formation/locality	Sample no.	Rock type	Group	Age in Ma
Middle Oxfordian	Punta Gruesa, S of Iquique	K30	Dacite, medium-K	**IV-2**	155
		K84	Andesite, high-K		
		K87	Dacite, medium-K		
Middle Oxfordian (Wittmann, 1999)	Los Tarros, SE of Arica	211	Andesite, medium-K	**IV-1**	155
		222	Andesite, medium-K		
Callovian/Oxfordian boundary (Kossler, 1998)	El Godo Fm., Coast, S of Iquique	K78	Basaltic Andesite, medium-K	**III-2**	157
		K79	Basaltic Andesite, high-K		
Callovian (Kossler, 1998)	El Godo Fm., Coast, S of Iquique	K28	Basaltic Andesite, low-K	**III-1**	159
		K29	Basaltic Andesite, low-K		163
Bathonian (Wittmann, 1999)	El Godo Fm., Coastal Range of Arica	244	Basaltic Andesite, medium-K		
		245	Basaltic Andesite, medium-K		
Late Early Bajocian (Kossler, 1998)	Caleta Ligate Fm., Coast, S of Iquique	K12	Basaltic Andesite, medium-K	**II**	171
		K16	Basalt, high-K		
		K45	Basaltic Andesite, high-K		
		K60	Basalt, high-K		
Early Bajocian to Lower Jurassic (Thomas, 1970, Kossler, 1998)	Oficina Viz Fm., Oficina Viz area, SE of Iquique	V6	Basaltic Andesite, high-K	**I**	175
		V9	Basaltic Andesite, high-K		
		V10	Basaltic Andesite, high-K		
		V14	Basaltic Andesite, medium-K		
		V15	Basaltic Andesite, medium-K		
		V21	Basaltic Andesite, medium-K		
Late Early to early Upper Bajocian (Gröschke & Wilke, 1986)	Western Cerro Jaspe, N of Chuquicamata	103	Alkaline Basalt	**V**	170
		105	Alkaline Basalt		
		108	Alkaline Basalt		

Classification of rocks according to Peccerillo and Taylor (1976) and Le Maitre et al. (1989).

SE-subduction of the Phoenix oceanic plate giving way to a sinistral transform offset (Jaillard et al., 1990). For matter of simplicity, we place the investigated volcanic rocks in five groups from different stratigraphic sections as shown in Table 1. The rock nomenclature generally follows that of the International Union of Geological Sciences Subcommission on the Systematics of Igneous Rocks (Le Maitre et al., 1989, see Table 1) unless otherwise stated.

The *Oficina Viz Formation southeast of Iquique* (group I) comprises thick basaltic andesitic and andesitic lava piles with a minimum thickness of 1500 m (Thomas, 1970), including flows up to 15 m thick and rare tuff layers. The abundance of pyroclastic interlayers increases towards the Caleta Ligate Formation, group II (Kossler, 1998). The subordinate pyroclastic rocks, the absence of pillow structures and quench textures, the brown to reddish brown color, and the intensive vesiculation of the Oficina Viz rocks point to subaerial eruption. Locally, dykes cut the lava piles. Their composition is similar to that of the lavas. The lavas are aphyric, pilitic, intersertal, and porphyric, and seriate porphyric due to plagioclase, clinopyroxene and/or tschermakite phenocrysts. To varying degrees, they are epidotized, sericitized, chloritized, or sometimes carbonatized. However, in many occurrences fresh clinopyroxene and amphibole phenocrysts are still preserved.

The Oficina Viz Formation is concordantly overlain by volcaniclastic rocks, limestones, and intercalated basaltic to basaltic andesititc lavas of the *Caleta Ligate Formation* (group II). These rocks are preserved along the coast south of Iquique and offshore. After a period of volcanic quiescence of about 6 Ma in the Iquique area (Kossler, 1998), tholeiitic and calc-alkaline basaltic andesites of the *El Godo Formation* (groups III-1 and III-2) were erupted. Both the Middle Jurassic Caleta Ligate and El Godo Formations are predominantly submarine deposits with pillow lavas, lava flows and intercalated volcaniclastic rocks, including dacitic to rhyolitic ignimbrites. These formations reach a total thickness of at least 600 m. Kossler (1998) documented by means of fine-laminated sediments and epibenthic fauna a deepening of the depositional environment from the Upper Bajocian to Callovian. The Caleta Ligate and El Godo Formations are cross-cut by mafic dykes. Rocks of both Formations display quench textures. The glassy groundmass and inclusions within phenocrysts are predominantly devitrificated and altered. Aphyric and intersertal to micro-ophitic textures predominate in the Caleta Ligate Formation, whereas porphyric textures characterize the volcanic rocks of the El Godo Formation.

Less altered basaltic andesitic to andesitic volcanic rocks (group III-1) of *Bathonian* age (according to Wittmann, 1999), which predominate in a volcano-sedimentary succession of 400 m minimum thickness at the coastal escarpment south of Arica, show structures and textures analogous to those of the El Godo Formation and are included into group III-1. Thick pillow piles indicate submarine depositional conditions for these rocks.

Amphibole-bearing (magnesiohornblende to tschermakite) andesitic to dacitic lava flows were found SSE of Arica at *Los Tarros* in the western Coastal Range (group IV-1). These rocks are amphibole- and feldspar-phyric with a hyalopilitic to trachytic groundmass. They represent Middle Oxfordian eruptions of less extensive

volcanic activities during the Upper Jurassic (Wittmann, 1999). Similar amphibole- and plagiophyric hyalopilitic but highly altered dacites are exposed at the shore of *Punta Gruesa* to the south of Iquique (group IV-2). They discordantly overlay the volcanic rocks of the El Godo Formation.

Alkaline basalts of the western *Cerro Jaspe* area (group V) are found as intercalations in Bajocian conglomerates, sandstones, and shallow water limestones (Gröschke and Wilke, 1986). The alkaline basalts contain fresh olivine and interstitial K-feldspar. The lavas show dominantly pillow and in part ropy pahoehoe structures reflecting submarine to terrestrial eruptive environments.

2.2. Biostratigraphic age of the volcanic rocks

The investigated Jurassic volcanic rocks are bracketed biostratigraphically, mainly by means of ammonites, over the Late Early Bajocian until the Middle Oxfordian (Gröschke and Wilke, 1986; Kossler, 1998; Wittmann, 1999). The volcanic rocks of the Oficina Viz Formation are assigned to the Bajocian. They are concordantly overlain by rocks of the Caleta Ligate Formation but it is unclear whether the Oficina Viz Formation continues into the Lower Jurassic. A Lower Jurassic volcanic activity is proved by pyroclastic deposits with Sinemurian Arietidae in the Iquique area (Kossler, 1998). The 6 Ma break of the volcanic activity throughout the uppermost Bajocian and Bathonian is indicated by Bivalvia of the Rotundum zone and the Ammonite Prohecticoceras (Kossler, 1998). For the Punta Gruesa volcanic rocks at the coast south of Iquique, Thomas (1970) assumed a Lower Cretaceous age. However, there is no biostratigraphic evidence for this epoch. Intermediate rocks from this locality have a similar petrographic (amphibole phenocrysts) and geochemical character as the Middle Oxfordian andesites and dacites of Arica. Therefore, we prefer to synchronize both occurrences and consider the Punta Gruesa volcanic rocks as Middle Oxfordian (about 155 Ma) in age.

The volcanic rocks investigated in this study cover a biostratigraphic age range of at least 20 Ma ($\geqslant$175–155 Ma). Close to the south of the study area, volcanic activity started already during the Upper Sinemurian (von Hillebrandt, 1996) and may have lasted about 40 Ma, from ~193 to ~155 Ma. This age range also corresponds to the time span of volcanic activity of the La Negra Formation in the Taltal-Copiapo region, south of our study area (Dallmeyer et al., 1996). Geochronological data (Grocott et al., 1994; Dallmeyer et al., 1996) confirm two distinct episodes of syn-extensional plutonism, during the Lower Jurassic (c. 202–188 Ma) and during the Upper Jurassic (ca. 160–153 Ma). These data show that the Jurassic volcanic activity in N-Chile occurred partly contemporaneous but mainly between these two phases of plutonism.

3. Analytical methods

Whole-rock data for major elements and some trace elements (Ba, Cr, Rb, Sr, Zr) were acquired by X-ray fluorescence (XRF) on glass fusion beads using a Philips

PW1404 automatic X-ray spectrometer. FeO has been determined by means of potentiometric titration following oxidizing decomposition. After catalytic combustion the H_2O and CO_2 contents were analyzed coulometrically with a limit of detection about 0.5 wt%. International and internal reference samples were used for calibration. Abundances of Cs, Cu, Ga, Hf, Li, Nb, Ni, Pb, Sc, Ta, Th, and U were determined by Inductively Coupled Plasma Mass Spectrometry (ICP-MS) using a VG Plasma Quad PQ^{2+} spectrometer. Relative standard deviation is less than $\pm 2\%$ for 12 runs of each sample and analytical accuracy is better than $\pm 10\%$ for each trace element. Rare Earth Element abundances (REE) and Y were analyzed by ICP-OES (Optical Emission Spectroscopy) with a Varian Liberty 200. Following sample fusion with sodium peroxide, the REEs were chromatographically separated and concentrated according to the procedure described by Zuleger and Erzinger (1988). Analytical accuracy is tested to be better than $\pm 10\%$.

For isotope analyses, samples were dissolved in 52% HF for 2–4 days at 160 °C on a hot plate. Digested samples were dried and redigested in 6 N HCl. Sr and Nd were separated and purified using standard ion exchange chromatography (Sr: Bio Rad AG50W-X8, 100–200 Mesh; Nd: HDEHP-coated Teflon powder). Pb was separated using the HBr–HCl ion-exchange procedure of Tilton (1973) and Manhès et al. (1978). Pb and Nd isotopic ratios were determined on a Finnigan MAT 262 multi-collector mass-spectrometer using static multicollection. Pb was measured from ~100 to 500 ng loads on single Re filaments and data were acquired at temperatures between 1180 and 1210 °C. Instrumental mass fractionation was corrected with 1.1‰ per a.m.u. based on the repeated measurement of NBS 981 Pb standard. Uncertainty of reported lead ratios is better than 0.1%. Nd samples were loaded with 0.1 M phosphoric acid on Ta filaments, and the measurements were performed using the double filament configuration with a Re ionization filament. $^{143}Nd/^{144}Nd$ ratios were normalized to $^{146}Nd/^{144}Nd = 0.7219$. Repeated measurements of the La Jolla Nd standard gave an average value 0.511910 ± 10 ($n = 6$). The measured $^{143}Nd/^{144}Nd$ ratios were adjusted to the value obtained in dynamic experiments (0.511850 ± 4, $n = 14$). The Sr isotope ratio measurements were carried out on a multi-collector Micromass SECTOR 54-30 mass spectrometer operated in dynamic mode. Sr was loaded with 1 M phosphoric acid on single Ta filaments. The $^{87}Sr/^{86}Sr$ ratios were normalized to $^{86}Sr/^{88}Sr = 0.1194$. Measurements of the NBS 987 Sr standard yielded 0.710246 ± 6 ($n = 8$). Uncertainties of $^{143}Nd/^{144}Nd$ and $^{87}Sr/^{86}Sr$ values are reported as $2\sigma_m$. Total procedural blanks during the measurement period were 30–50 pg for Pb, < 100 pg for Sr, and < 50 pg for Nd.

4. Results

4.1. Major and trace element distribution

The major and trace element compositions of selected samples are discussed with respect to the five groups named above (Table 1). For graphical presentation of

element distributions and geochemical rock classification, extended normalized trace element patterns in the order of decreasing incompatibility have been used (Fig. 2).

The spidergrams in Fig. 2a display negative Nb–Ta–P–Ti anomalies for the volcanic rocks of the Oficina Viz Formation (group I), El Godo Formation (group III), and Oxfordian (group IV). Weak negative or no Nb–Ta–Ti anomalies exist for the Caleta Ligate volcanics (group II). The alkaline basalts from Cerro Jaspe (group V) are characterized by positive Nb–Ta–Ti anomalies. Compared to the other groups, the pattern of the less incompatible elements Th to Lu of samples from the Caleta Ligate group and the Co. Jaspe alkaline basalts show very little variation. The pattern of groups I and III volcanic rocks are subparallel. Their trace element content varies by a factor of 2–3 (Fig. 2a). Large ion lithophile (LIL)-elements scatter throughout all groups. Eu-anomalies occur only in groups I and III, whereas both, positive and negative Sr-anomalies are common in all volcanic rocks from the coastal range (groups I–IV).

In order to illustrate the within-group variance caused by magma generation and evolution and/or rock alteration, we have normalized the data of each group to the sample having the lowest degree of alteration (Fig. 2b), which was evaluated by means of alteration mineral assemblages as well as H_2O^+- and CO_2-contents (Table 2). Elements susceptible to secondary low-T alteration scatter widely (e.g., Rb, Cs, Pb), whereas less mobile elements, such as Th, Nb, Ta, and REE generally show coherent patterns. If, for example, the CO_2-bearing samples K16, K78, and 103 with the other samples in their groups are compared, we find no striking differences between immobile incompatible element contents. This justifies to discuss their petrogenetic fingerprint.

Rocks of the Cerro Jaspe series (group V) show a small range in major element composition and their trace element patterns display no variation apart from scatter in the alkali and alkaline-earth elements. Rocks of the Caleta Ligate Formation (group II) also have a rather narrow range in major element composition. Their patterns of immobile trace elements display small variations of Th, Nb, Ta, LREE, and Ti. The remaining three groups have a broader range in major element composition (e.g., $Mg\# = 100Mg/(Mg + Fe_{tot}) = 42–69$) compared to rocks from groups II and V. They show heterogeneous normalized patterns, most distinctive in the parallel offset of the pattern in rocks of the El Godo Formation (group III, Fig. 2b). Two samples of the El Godo Formation show distinctly lower trace element contents and distinct positive Sr anomalies. Rocks of the Oficina Viz Formation (group I), which encompass a large compositional range ($Mg\# = 44–64$), display scattered but roughly subparallel pattern for immobile trace elements. This group splits up into two subgroups, the one characterized by positive Sr anomaly and low-HREE contents, the other by negative Sr anomaly and higher REE values.

An extended data set for the groups I–IV is plotted in binary diagrams with Zr as parameter of differentiation according to MacLean and Barret, 1993; Fig. 3d). The Oficina Viz samples show positive correlation and the largest range of elemental variation in the Ti- and Y-diagrams. The group IV rocks define separated fields with

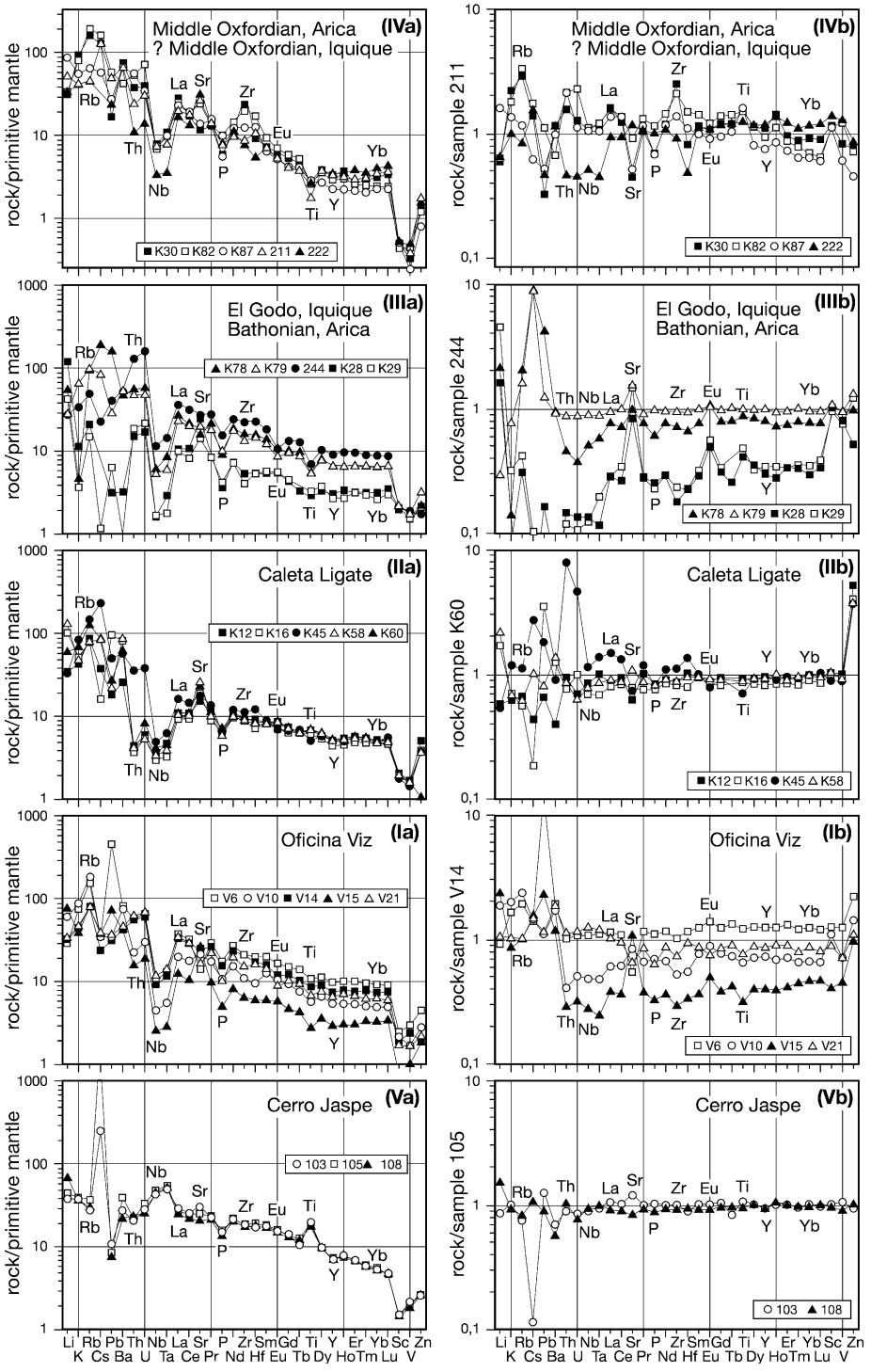
Middle Oxfordian, Arica
? Middle Oxfordian, Iquique
(IVa)
(IVb)
El Godo, Iquique
Bathonian, Arica
(IIIa)
(IIIb)
Caleta Ligate
(IIa)
(IIb)
Oficina Viz
(Ia)
(Ib)
Cerro Jaspe
(Va)
(Vb)
rock/primitive mantle
rock/sample 211
rock/sample 244
rock/sample K60
rock/sample V14
rock/sample 105
K30 K82 K87 211 222
K78 K79 244 K28 K29
K12 K16 K45 K58 K60
V6 V10 V14 V15 V21
103 105 108
Li Rb Pb Th Nb La Sr P Zr Sm Gd Ti Y Er Yb Sc Zn
K Cs Ba U Ta Ce Pr Nd Hf Eu Tb Dy Ho Tm Lu V

low Ti and Y concentrations. The group II rocks scatter within the low-Zr and most of the basaltic andesites of group III within the high-Zr range.

Data in Table 2 and Figs. 2, 3, and 6 demonstrate that each group of volcanic rocks, originally classified on stratigraphical and petrographical reasons, has its own geochemical character. For example, the average La/Yb ratios vary from 6.5 (group I), 3.4 (group II), 5.5 (group III) and finally increase up to 11.7 (group IV). A similar trend is also apparent for the Ta/Yb- and Zr/Y-ratios (Table 2). Alkaline basalts of group V differ from all other investigated rocks by higher Ta/Sm (0.26) and Ta/Yb (0.81) and significantly lower Th/Ta ratios (1.0).

With the exception of sample K45, group II lavas and samples K28 and K29 of group III have very low-Ta/Yb ratios (0.08), ΣLREE (37.6), and comparatively low-Zr/Y ratios. They plot in the tholeiite field (Fig. 3c). This is compatible with their higher Mg#-values of 53–69 (see Gill, 1981). Typically, the basaltic andesites and andesites, (groups I, III, and IV) are enriched in LILE such as Ba and Th, and in LREE, but depleted in high field strength elements (HFSE) such as Nb, Ta, and Ti. Some samples of groups I and III-1, and the entire group IV have low HREE between 4.1 to 6.8 ppm (Table 2).

The main part of the investigated volcanic rocks suffered a certain alteration. Therefore, we verify the result of the main element classification after Le Maitre et al. (1989), see Table 1, by discrimination in a Zr/TiO_2 vs. Nb/Y diagram according to Winchester and Floyd (1977). This immobile element diagram (Fig. 4) discriminates the Jurassic alkaline basalts from the basalt and basaltic andesites and the latter from both andesites and dacites.

4.2. Isotopic compositions

The isotopic compositions of all samples were corrected for post-crystallization in situ growth of radiogenic Sr, Nd, and Pb. The Sr and Nd isotopic compositions are given in Table 3 and plotted in Fig. 5. εNd_i-values of the tholeiitic and alkaline mafic rocks (groups II and V) display a range from 7.1 to 4.8, whereas the more evolved samples of these groups have values between 2.2 and 5.9 (Fig. 5a). The $^{87}Sr/^{86}Sr_i$ values fall in the range 0.7032–0.7056. The $^{87}Sr/^{86}Sr_i$ ratios of groups I, II, and V plot in small ranges (0.7036–0.7041, 0.7040–0.7043, and 0.7036–0.7038, respectively). Amphibole-bearing rocks of the groups I and IV join in a field with the lowermost $^{87}Sr/^{86}Sr_i$ ratios (Fig. 5a). The most samples fall within the Sr–Nd mantle array (DePaolo and Wasserburg, 1979).

Initial lead isotopic ratios of most samples plot in narrow ranges from 18.27 to 18.42 ($^{206}Pb/^{204}Pb_i$), 15.58 to 15.63 ($^{207}Pb/^{204}Pb_i$), and from 38.12 to 38.30

Fig. 2. Normalized element distribution diagrams of volcanic rocks from the Jurassic arc and back arc area. (a) Extended incompatible element pattern with primitive mantle normalization according to Hofmann (1988). See the two branches of the Oficina Viz curves in the HREE section. (b) Incompatible element pattern like in Fig. 2a, but each group normalized by a reference sample having the lowest degree of alteration.

Table 2. Main and trace element chemistry of Jurassic mafic to intermediate volcanic rocks from North Chilean Coastal Range and Cerro Jaspe (oxides in wt.%, trace elements in ppm)

Group	Group I						Group II				Group III-1	
Sample	V6	V14	V15	V21	La2	Vz8	K12	K16	K45	K60	K28	K29
SiO_2	52.3	53.2	54.6	55.4	53.5	48.4	51.2	46.1	54.5	49.0	52.9	51.5
TiO_2	1.91	1.54	0.51	1.19	0.92	0.70	1.16	1.04	0.87	1.26	0.50	0.58
Al_2O_3	13.6	16.1	18.9	15.9	17.6	18.7	16.8	16.4	17.1	17.2	16.1	18.6
Fe_2O_3	8.99	5.04	4.41	4.70	5.94	2.76	2.86	6.07	2.29	7.04	2.33	3.40
FeO	3.50	4.51	3.12	3.28	0.60	4.97	4.61	2.13	3.97	2.39	3.95	2.86
MnO	0.31	0.15	0.14	0.14	0.15	0.15	0.64	0.21	0.19	0.15	0.15	0.11
MgO	5.14	4.31	3.77	4.84	5.88	7.47	4.62	4.58	4.58	5.96	7.53	6.13
CaO	5.28	8.67	6.52	7.92	6.42	8.10	8.39	11.8	6.45	7.18	6.43	5.18
Na_2O	3.36	3.09	4.15	2.83	5.07	3.03	4.50	3.37	4.12	4.26	6.11	5.89
K_2O	2.32	1.35	1.22	1.45	1.60	1.42	1.26	1.53	2.56	2.13	0.10	0.33
P_2O_5	0.38	0.32	0.11	0.22	0.20	0.090	0.13	0.12	0.13	0.15	0.085	0.076
H_2O^+	2.96	1.92	2.76	1.98	2.56	3.42	2.66	3.18	2.41	2.47	3.25	4.53
CO_2	0.13	0.09	0.16	0.19	0.12	0.13	1.32	2.87	0.93	0.99	1.11	0.20
Total	100.3	100.3	100.5	100.0	100.7	99.3	100.2	99.4	100.1	100.2	100.6	99.4
Mg#	44.1	45.9	48.7	53.5	63.8	64.0	53.1	53.4	57.5	54.9	68.9	64.9
Li	24	26	64	28	46	55	29	86	27	50	35	97
Rb	81	43	43	43	45	47	47	40	79	71	8	11
Cs	0.97	0.64	1	1.1	4.1	5.8	1	0.43	6.2	2.3	0.03	0.06
Pb	79	5.4	13	6.4	9.5	3.1	3.2	17	8.8	4.9	1.1	0.55
Ba	502	256	315	279	125	212	158	502	348	393	6	19
Th	4.5	4.4	1.3	5.1	1.1	0.93	0.35	0.29	2.9	0.37	1.5	1.2
U	1.3	1.2	0.39	1.4	0.28	0.24	0.12	0.17	0.78	0.17	0.44	0.34
Nb	6.1	5.6	1.6	7.2	6.7	1.2	2.2	1.8	3	2.6	1	0.93
Ta	0.45	0.4	0.1	0.49	0.45	0.11	0.16	0.11	0.22	0.16	0.06	0.1
Sr	252	455	510	303	640	809	279	342	323	440	259	449
Zr	208	202	62	151	115	50	85	81	108	98	39	51
Hf	5.3	4.6	1.6	4.4	3	1	2.4	1.9	3.2	2.4	1.4	1.4
Sc	37	29	12	26	18	32	31	30	26	30	30	27
V	377	300	136	217	114	196	211	202	181	212	190	172
Cr	8	43	11	86	139	63	241	236	70	273	305	105
Ni	9.8	21	6.2	29	86	42	113	62	46	105	99	58
Zn	220	98	94	109	77	58	253	195	181	50	43	103
Th/Ta	10	11	13	10	2.4	8.4	2.2	2.6	13	2.3	25	12
Ta/Yb	0.12	0.13	0.07	0.19	0.3	0.08	0.08	0.06	0.10	0.08	0.05	0.08
Th/U	3.5	3.7	3.3	3.6	3.9	3.9	2.9	1.7	3.7	2.2	3.4	3.5
Ta/Sm	0.058	0.065	0.043	0.089	0.11	0.044	0.050	0.034	0.065	0.047	0.030	0.045
Zr/Y	5.6	7.0	5.2	6.0	7.7	3.8	4.3	4.8	5.4	4.7	3.7	4.3
Ba/La	21.8	12.8	40.4	13.3	8.3	37.2	25.9	89.6	34.8	57.0	1.0	3.0
La/Sr	0.091	0.044	0.015	0.069	0.023	0.007	0.022	0.016	0.031	0.016	0.024	0.014
Sr/Y	6.8	15.7	42.5	12.1	42.7	62.2	14.0	20.1	16.2	21.0	24.7	37.4
Y	37	29	12	25	15	13	20	17	20	21	10.5	12
La	23	20	7.8	21	15	5.7	6.1	5.6	10	6.9	6.2	6.4
Ce	52	46	17	45	35	14	17	15	24	18	13	17
Pr	7.1	6.2	2.4	5.4	4.8	2.0	2.8	2.1	3.3	2.8	2	1.9
Nd	32	27	10	24	20	9.0	12	11	14	13	8.5	8.5
Sm	7.8	6.2	2.3	5.5	4.0	2.5	3.2	3.2	3.4	3.38	2.02	2.2
Eu	2.4	2	0.85	1.3	1.3	0.91	1.2	1.1	1	1.3	0.74	0.82

Table 2. (*continued*)

Group	Group I						Group II				Group III-1	
Sample	V6	V14	V15	V21	La2	Vz8	K12	K16	K45	K60	K28	K29
Gd	7.6	6.1	2.4	5.2	3.4	2.5	3.7	3.2	3.5	3.9	2.1	2.3
Tb	1.3	0.96	0.41	0.88	0.54	0.38	0.59	0.59	0.64	n.d.	0.3	n.d.
Dy	7.2	5.7	2.3	5	3.0	2.5	3.8	3.4	3.7	4.1	2.3	2.1
Ho	1.4	1.1	0.44	1	0.56	0.48	0.77	0.65	0.69	0.77	0.38	0.47
Er	4.1	3.1	1.3	2.8	1.6	1.5	2.3	2	2.3	2.4	1.3	1.3
Tm	0.6	0.49	0.22	0.39	0.24	0.22	0.35	0.3	0.35	0.37	0.19	0.2
Yb	3.8	3	1.4	2.6	1.5	1.3	2.1	1.9	2.1	2.13	1.1	1.3
Lu	0.57	0.47	0.22	0.38	0.23	0.20	0.31	0.29	0.35	0.34	0.19	0.22
ΣREE	151	128	49	120	88	43	56	50	69	59	40	45
ΣLREE	114	99	37	95	75	31	38	34	51	41	30	34
ΣMREE	19	15	6.0	13	6.2	6.3	8.7	8.1	9.5	8.6	5.2	5.3
ΣHREE	18	14	5.9	12	7.1	6.2	9.6	8.5	9.5	10	5.5	5.6
La/Yb	6.0	6.7	5.6	8.1	10	4.4	2.9	3.0	4.8	3.2	5.6	4.9
La/Sm	3.3	8.7	1.4	2.9	3.8	2.3	1.9	1.6	3.0	0.9	2.8	2.0

Group	Group III-1		Group III-2		Group IV-1		Group IV-2			Group V		
Sample	244	245	K78	K79	211	222	K30	K84	K87	103	105	108
SiO_2	53.4	53.2	51.9	53.4	61.2	59.8	63.9	59.3	64.9	43.8	45.6	44.9
TiO_2	1.20	1.18	0.98	0.99	0.33	0.40	0.49	0.60	0.51	3.54	3.50	3.43
Al_2O_3	16.6	16.3	17.2	16.7	18.4	18.5	16.3	17.3	15.4	13.9	14.2	14.0
Fe_2O_3	5.29	4.42	0.22	4.62	3.13	3.36	2.29	3.94	4.33	10.3	7.02	5.84
FeO	3.42	4.45	5.61	3.20	1.65	1.85	1.37	b.l.	b.l.	1.80	5.77	6.66
MnO	0.12	0.14	0.080	0.17	0.15	0.16	0.086	0.047	0.070	0.12	0.17	0.17
MgO	3.37	4.09	1.86	4.66	2.04	2.18	2.33	0.25	1.03	4.81	8.10	7.95
CaO	9.04	8.75	11.0	7.84	4.35	5.07	2.07	3.05	1.47	11.2	7.92	7.08
Na_2O	3.23	3.16	3.12	3.68	5.04	4.83	5.00	6.55	7.68	2.59	3.54	3.38
K_2O	1.01	0.79	1.15	2.02	1.30	1.28	2.74	5.78	1.69	1.16	1.19	1.18
P_2O_5	0.33	0.33	0.19	0.21	0.18	0.18	0.12	0.20	0.12	0.34	0.34	0.31
H_2O^+	2.73	2.73	2.37	1.76	1.98	1.91	2.22	0.48	1.13	2.96	2.83	3.78
CO_2	0.28	0.17	4.24	0.79	0.11	0.29	0.47	2.10	1.09	3.00	0.11	0.33
Total	100.0	99.7	99.9	100.0	99.9	99.8	99.4	99.6	99.4	99.6	100.3	99.0
Mg#	42.3	46.4	36.3	53.0	44.9	44.4	54.8	11.2	32.0	43.8	54.4	54.3
Li	22	6.6	47	24	44	29	26	1.8	70	32	37	59
Rb	26	43	53	57	30	25	85	173	34	15	20	17
Cs	0.58	49	5.2	2.3	2.5	3.9	3.4	1.3	1.5	6.5	58	65
Pb	6.9	8.8	29	5.2	9.1	4.3	2.9	6.8	4.7	1.9	1.5	1.4
Ba	307	310	296	334	388	457	445	819	378	166	242	142
Th	10.2	9	4.6	4	2	0.93	3.1	4.4	4.3	1.7	1.9	2
U	3.2	2.8	1.2	1	0.63	0.29	0.8	1.3	0.69	0.58	0.68	0.54
Nb	7.5	6.8	3.8	3.3	4.1	2.1	4.2	4.8	4.2	27	30	29
Ta	0.52	0.46	0.3	0.21	0.29	0.13	0.34	0.38	0.3	1.8	1.9	1.9
Sr	308	480	298	369	488	580	214	108	247	561	463	399
Zr	219	207	156	132	87	78	214	162	118	193	192	181
Hf	6.3	5.9	4.1	3.9	3.1	1.5	2.5	5	3.3	4.7	3.5	5.1
Sc	29	29	31	33	6.5	8.7	7.6	7.7	7.4	23	23	23
V	234	235	224	229	52	66	42	63	30	282	268	250
Cr	30	54	47	98	b.l.	b.l.	20	30	18	214	226	220

Table 2. (*continued*)

Group	Group III-1		Group III-2		Group IV-1		Group IV-2			Group V		
Sample	244	245	K78	K79	211	222	K30	K84	K87	103	105	108
Ni	14	18	26	20	4.6	3.8	9.4	8.3	8.5	74	86	88
Zn	86	84	111	162	90	76	65	63	39	128	136	140
Th/Ta	19.6	19.6	15.3	19.0	6.9	7.2	9.1	11.6	14.3	0.9	1.0	1.1
Ta/Yb	0.14	0.12	0.10	0.08	0.20	0.08	0.26	0.32	0.33	0.78	0.83	0.83
Th/U	3.2	3.2	3.8	4.0	3.2	3.2	3.9	3.4	6.2	2.9	2.8	3.7
Ta/Sm	0.074	0.067	0.057	0.043	0.11	0.046	0.12	0.10	0.12	0.25	0.26	0.28
Zr/Y	6.1	5.9	5.6	4.9	7.3	5.6	16.5	12.5	13.6	6.9	6.4	6.2
Ba/La	14.0	14.8	17.4	22.9	36.6	45.7	34.2	48.2	27.0	9.2	14.2	8.9
La/Sr	0.071	0.044	0.057	0.040	0.022	0.017	0.061	0.157	0.057	0.032	0.037	0.040
Sr/Y	8.6	13.7	10.6	13.7	40.7	41.4	16.5	8.3	28.4	20.0	15.4	13.8
Y	36	35	28	27	12	14	13	13	8.7	28	30	29
La	22	21	17	14.6	10.6	10	13	17	14	18	17	16
Ce	50	49	36	34	23	22	28	36	30	41	40	37
Pr	6.9	6.4	5.3	4.5	3.1	3.2	3.3	4.3	3.5	5.8	5.8	5.5
Nd	29	28	22	21	12	13	14	18	14	27	27	26
Sm	7	6.9	5.3	4.9	2.61	2.8	2.9	3.8	2.5	7.2	7.2	6.9
Eu	1.5	1.5	1.6	1.3	0.86	0.93	0.91	1.1	0.76	2.4	2.4	2.3
Gd	6.9	6.8	5.3	5.1	2.3	2.7	2.7	3.3	2.1	7.5	7.2	7.2
Tb	1.2	1.2	0.95	0.82	0.37	0.44	0.43	0.51	0.37	1.02	1.22	1.22
Dy	6.6	6.5	5.3	5.1	2.2	2.5	2.4	2.6	1.7	6.4	6.3	6.5
Ho	1.4	1.3	1	0.96	0.38	0.50	0.52	0.52	0.31	1.1	1.1	1.2
Er	4	3.8	3	2.9	1.3	1.6	1.2	1.1	0.9	2.9	2.9	3
Tm	0.58	0.58	0.45	0.45	0.21	0.23	0.18	0.19	0.13	0.37	0.39	0.39
Yb	3.8	3.7	2.9	2.77	1.46	1.7	1.3	1.2	0.91	2.3	2.3	2.3
Lu	0.58	0.55	0.44	0.44	0.24	0.28	0.21	0.17	0.14	0.3	0.31	0.32
ΣREE	141	137	106	99	61	62	71	90	71	123	121	116
ΣLREE	108	104	80	74	49	48	58	75	62	92	90	84
ΣMREE	16.6	16.4	13.2	12.6	6.14	6.87	6.94	8.71	5.73	18.1	18.0	17.6
ΣHREE	17.0	16.4	13.1	12.6	5.79	6.81	5.81	5.78	4.09	13.4	13.3	13.7
La/Yb	5.8	5.7	5.9	5.3	7.3	5.9	10	14	15	7.8	7.4	7.0
La/Sm	3.2	10	3.5	2.1	3.8	1.9	3.6	6.8	5.4	2.5	2.5	2.3

b.l.—below limit of detection; n.d.—non determined.
Analytical methods see in the text, sample localities in Table 1.

($^{208}Pb/^{204}Pb_i$), Fig. 5b. The two alkali basalts from group V and three basaltic andesites from group III are characterized by low isotope ratios in the range 18.22–18.31 for $^{206}Pb/^{204}Pb_i$, 15.58–15.61 for $^{207}Pb/^{204}Pb_i$, and 38.08–38.18 for

Fig. 3. (Ti, Cr, Y) vs. Zr plots of Jurassic volcanic rocks. (a–c): Linear correlations, d: logarithmic correlation (log Cr–log Zr diagram). 1 and 1a are mixing or fractionation trend lines or curves. 2 and 3 connect samples of the same stratigraphic unit. THOL—tholeiitic, TRANS—transitional, and CALCALK—calc-alkaline fields according to MacLean and Barret (1993) in the Y–Zr diagram. The samples are marked by sample number or enlarged symbols, if investigated for isotope composition.

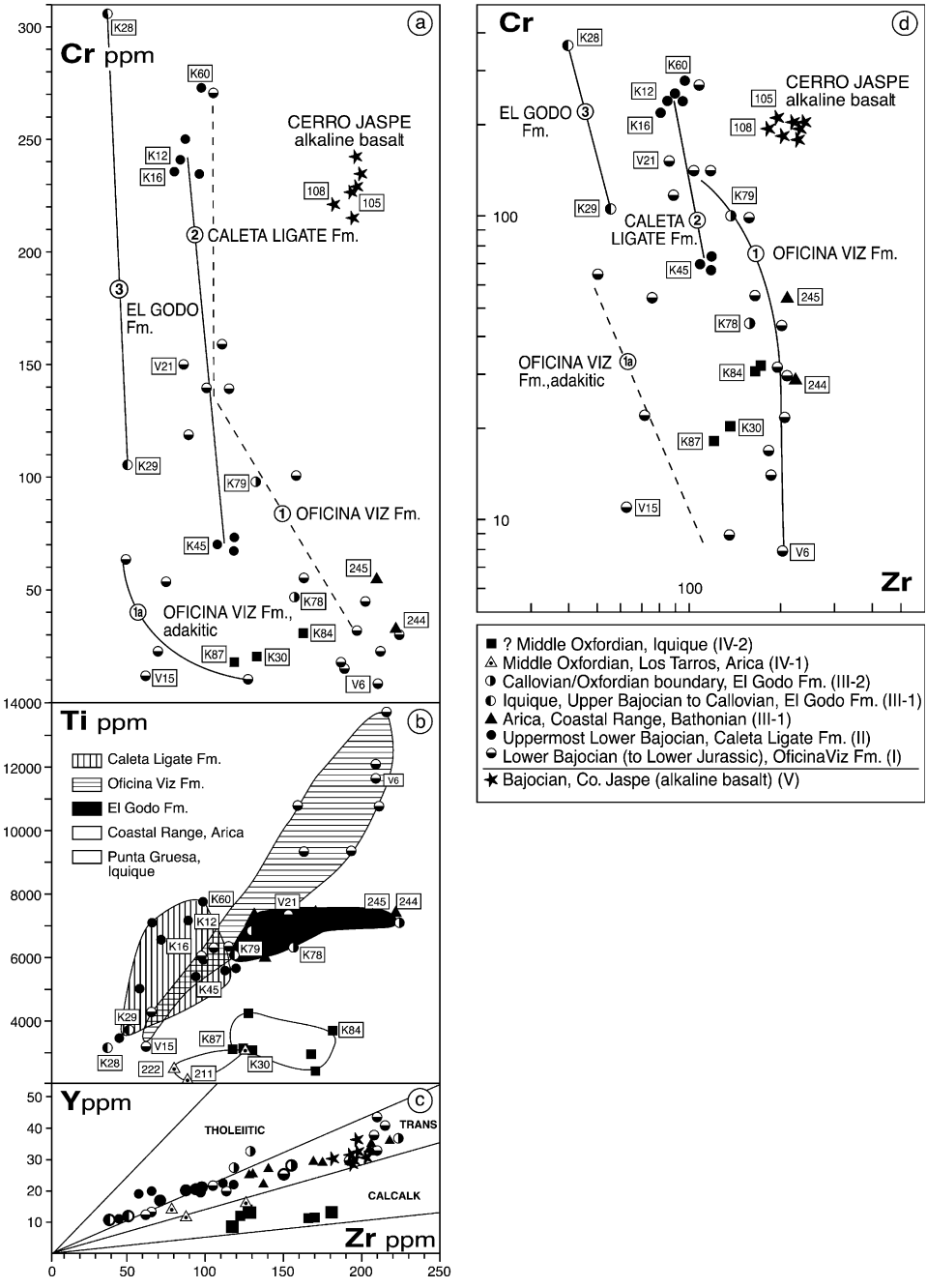
a
Cr ppm
CERRO JASPE
alkaline basalt
② CALETA LIGATE Fm.
③ EL GODO Fm.
① OFICINA VIZ Fm.
1a OFICINA VIZ Fm., adakitic
b
Ti ppm
Caleta Ligate Fm.
Oficina Viz Fm.
El Godo Fm.
Coastal Range, Arica
Punta Gruesa, Iquique
c
Yppm
THOLEIITIC
TRANS
CALCALK
Zr ppm
d
Cr
Zr
■ ? Middle Oxfordian, Iquique (IV-2)
△ Middle Oxfordian, Los Tarros, Arica (IV-1)
◑ Callovian/Oxfordian boundary, El Godo Fm. (III-2)
◐ Iquique, Upper Bajocian to Callovian, El Godo Fm. (III-1)
▲ Arica, Coastal Range, Bathonian (III-1)
● Uppermost Lower Bajocian, Caleta Ligate Fm. (II)
◒ Lower Bajocian (to Lower Jurassic), OficinaViz Fm. (I)
★ Bajocian, Co. Jaspe (alkaline basalt) (V)

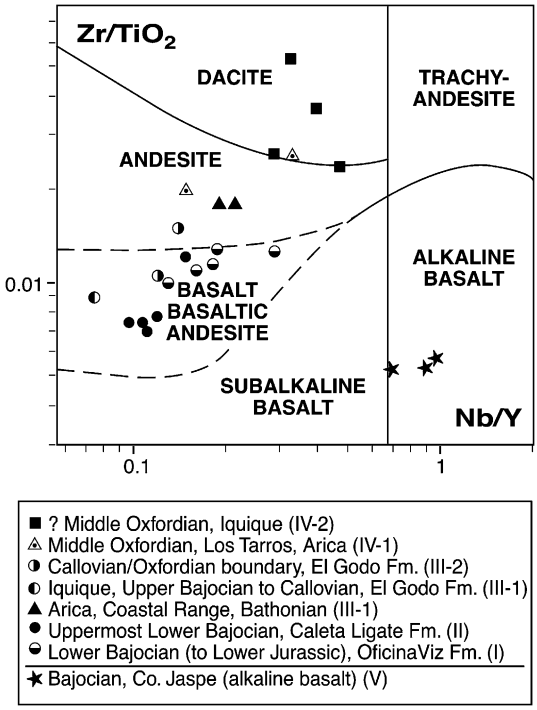

Fig. 4. Zr/TiO_2 vs. Nb/Y discrimination diagram according to Winchester and Floyd (1977).

$^{208}Pb/^{204}Pb_i$. The andesite sample from group I shows slightly more radiogenic Pb isotope compositions.

5. Discussion

The chemical and Sr–Nd isotope signatures of the mafic to intermediate Jurassic volcanic rocks from N-Chile, clearly document a strong input of mantle material. However, indicated by low Mg#, Cr, and Ni contents none of the investigated samples represent primary mantle melt composition. To distinguish between different mantle and slab components involved in the generation of these rocks, it must first be assured, that the variability in chemical composition does not originate to a significant extend from contamination by continental crustal material. Such contamination could be derived from subducted sedimentary material in the magma source or from assimilation of crustal material during magma ascent and magma evolution. Thus, in Section 1, we assess the magnitude of contribution of crustal material to identify the least affected samples. In Section 2, the magma source of these samples is discussed in terms of controlling reservoirs and finally in terms of geographical and temporal distribution of melting in a regional tectonic setting.

Table 3. Sr, Nd and Pb isotopic composition of Jurassic mafic to intermediate volcanic rocks from North Chile

Sample	Rock type	Age (Ma)[a]	$^{87}Sr/^{86}Sr$[b]	$^{87}Sr/^{86}Sr_i$[c]	$^{143}Nd/^{144}Nd$[b]	εNd[d]	εNd_i[c,d]	$^{206}Pb/^{204}Pb$[e]	$^{206}Pb_i/^{204}Pb$[f]	$^{207}Pb/^{204}Pb$[e]	$^{207}Pb_i/^{204}Pb$[f]	$^{208}Pb/^{204}Pb$[e]	$^{208}Pb_i/^{204}Pb$[f]
K30	Dacite	155	0.706615 (8)	0.70405	0.512744 (6)	2.07	3.5	18.856	18.43	15.647	15.63	38.842	38.30
K84	Andesite	155	0.713031 (8)	0.70322	0.512867 (9)	4.47	6.0	18.660	18.36	15.623	15.61	38.580	38.25
K87	Dacite	155	0.704404 (8)	0.70349	0.512793 (11)	3.02	4.8	18.634	18.41	15.621	15.61	38.666	38.20
211	Andesite	155	0.704604 (8)	0.70421	0.512772 (8)	2.61	3.9	18.498	18.39	15.614	15.61	38.415	38.30
222	Andesite	155	0.704426 (8)	0.70411	0.512801 (12)	3.18	4.1	18.495	18.39	15.604	15.60	38.368	38.26
K78	Bas. Andesite	157	0.704705 (8)	0.70353	0.512824 (7)	3.63	4.7	18.444	18.38	15.616	15.61	38.375	38.29
K79	Bas. Andesite	157	0.704651 (8)	0.70363	0.512871 (6)	4.55	5.7	18.578	18.28	15.614	15.60	38.532	38.14
K28	Bas. Andesite	159	0.705828 (9)	0.70562	0.512880 (8)	4.72	5.9	20.402	(19.75)	15.705	(15.67)	38.695	(37.97)
K29	Bas. Andesite	159	0.704911 (8)	0.70474	0.512845 (6)	4.04	4.9	19.069	(18.07)	15.621	(15.57)	38.951	(37.80)
244	Bas. Andesite	163	0.705761 (8)	0.70512	0.512693 (6)	1.07	2.2	18.985	18.22	15.649	15.61	38.978	38.18
245	Bas. Andesite	163	0.705319 (8)	0.70466	0.512759 (6)	2.36	3.8	18.798	18.28	15.617	15.59	38.718	38.17
K12	Bas. Andesite	171	0.705215 (8)	0.70401	0.512921 (6)	5.52	6.3	18.434	18.37	15.614	15.61	38.331	38.27
K16	Basalt	171	0.705174 (15)	0.70434	0.512863 (5)	4.39	4.9	18.421	18.40	15.607	15.61	38.303	38.29
K45	Bas. Andesite	171	0.705866 (8)	0.70411	0.512825 (6)	3.65	4.8	18.483	18.27	15.602	15.59	38.375	38.12
K60	Basalt	171	0.705291 (8)	0.70413	0.512922 (6)	5.54	6.4	18.438	18.38	15.609	15.61	38.310	38.27
V6	Bas. Andesite	175	0.705983 (8)	0.70365	0.512872 (15)	4.56	5.6	18.496	18.47	15.640	15.64	38.476	38.44
V15	Bas. Andesite	175	0.704523 (10)	0.70391	0.512737 (5)	1.93	3.2	18.457	18.41	15.607	15.60	38.344	38.29
V21	Bas. Andesite	175	0.705145 (10)	0.70412	0.512689 (8)	0.99	2.3	18.762	18.38	15.623	15.60	38.707	38.25
105	Alkaline Basalt	170	0.703930 (8)	0.70362	0.512876 (6)	4.64	5.4	19.090	18.31	15.635	15.60	38.815	38.10
108	Alkaline Basalt	170	0.704248 (8)	0.70385	0.512960 (5)	6.28	7.1	18.961	18.30	15.608	15.58	38.866	38.07

[a]Ages based on biostratigraphy cited in Table 1, and Mesozoic time scale from Pálfy et al. (2000).

[b]Uncertainties (in brackets) are $\pm 2\sigma_m$ within-run precision and refer to the last digits.

[c]Initial composition recalculated using Rb, Sr and Sm, Nd concentrations as determined by XRF and ICP-OES, respectively with $\lambda^{87}Rb = 1.42 \times 10^{-11}$ and $\lambda^{147}Sm = 6.54 \times 10^{-12}\,y^{-1}$.

[d]εNd and εNd_i calculated using chondritic reference (CHUR) with present-time parameters $^{143}Nd/^{144}Nd = 0.512638$ and $^{147}Sm/^{144}Nd = 0.1967$.

[e]Corrected for mass fractionation with 0.11%/a.m.u. based on repeated measurements of the NBS 981 Pb standard; 2σ confidence level is better than 0.1%.

[f]Initial composition recalculated using the Th, U and Pb concentrations determined by ICP-MS. Values in parentheses appear anomalous and may reflect subrecent mobility of U and Pb.

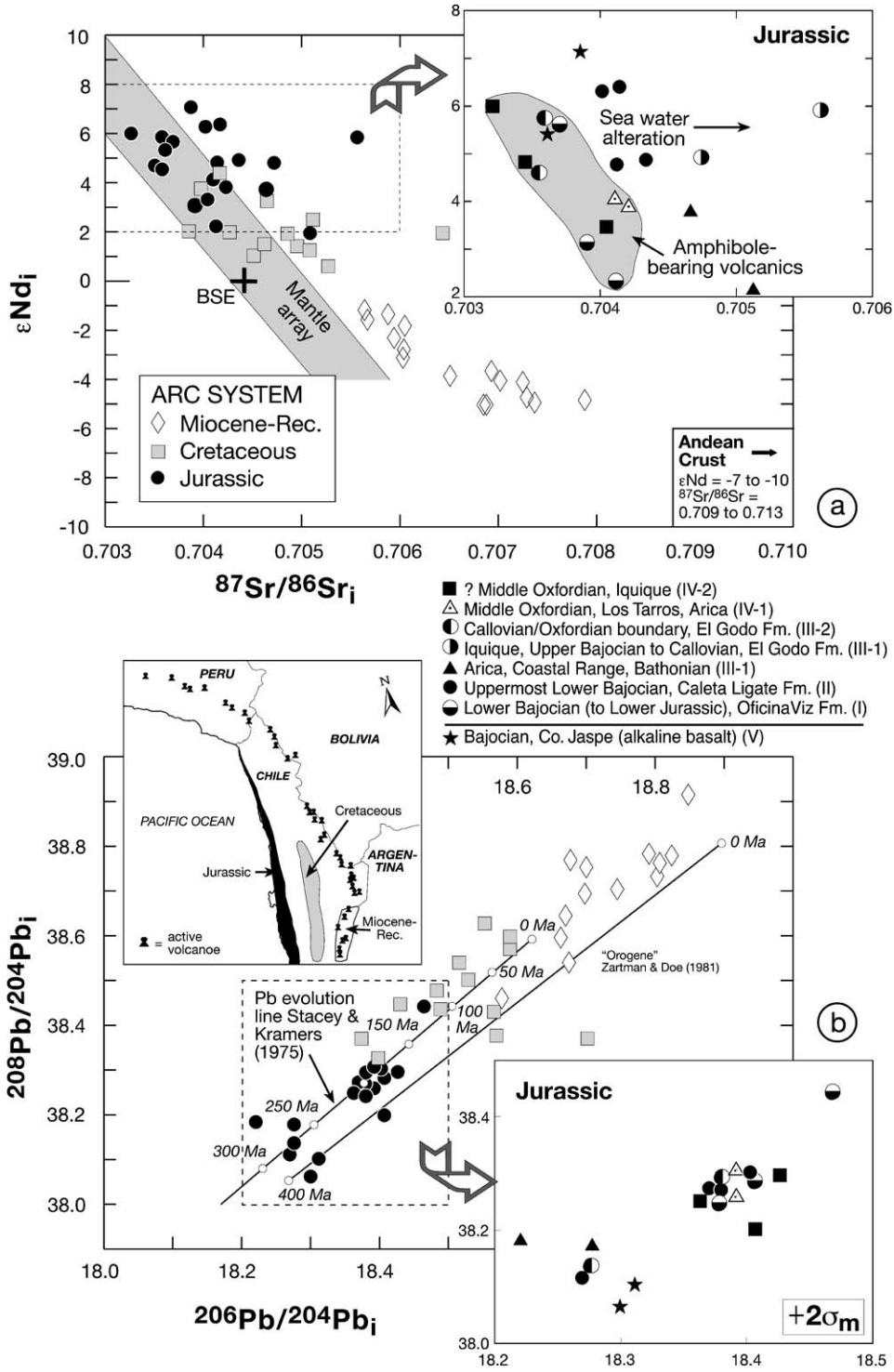
Jurassic
Sea water alteration
Amphibole-bearing volcanics
BSE
Mantle array
ARC SYSTEM
Miocene-Rec.
Cretaceous
Jurassic
Andean Crust
εNd = -7 to -10
87Sr/86Sr = 0.709 to 0.713
a
εNdi
87Sr/86Sri
? Middle Oxfordian, Iquique (IV-2)
Middle Oxfordian, Los Tarros, Arica (IV-1)
Callovian/Oxfordian boundary, El Godo Fm. (III-2)
Iquique, Upper Bajocian to Callovian, El Godo Fm. (III-1)
Arica, Coastal Range, Bathonian (III-1)
Uppermost Lower Bajocian, Caleta Ligate Fm. (II)
Lower Bajocian (to Lower Jurassic), OficinaViz Fm. (I)
Bajocian, Co. Jaspe (alkaline basalt) (V)
PERU
BOLIVIA
CHILE
PACIFIC OCEAN
Cretaceous
Jurassic
ARGEN-TINA
Miocene-Rec.
= active volcanoe
Pb evolution line Stacey & Kramers (1975)
0 Ma
50 Ma
100 Ma
150 Ma
250 Ma
300 Ma
400 Ma
"Orogene" Zartman & Doe (1981)
b
Jurassic
+2σm
208Pb/204Pbi
206Pb/204Pbi

5.1. Crustal contributions and the isotopic signature of the Central Andean crust

The isotopic systems of Pb, Sr and Nd react differently during mantle–crust interaction depending on the contrasts of their isotopic signatures and concentrations. As mantle rocks and mantle-derived rocks generally contain very low total Pb contents, i.e., typically 15–100 times lower than average crustal rocks (e.g., Sun, 1980; Weaver and Tarney, 1980; Zindler and Hart, 1986), even small amounts of crustal rocks assimilated into mantle-derived melts can cause a significant change in Pb isotope composition. Enriched subcontinental mantle or subducted terrigenous sediments, however, may not differ isotopically from the crustal component. Compared to Pb, Sr is less sensitive to crustal assimilation as concentration of Sr contrasts between mantle and crust are less pronounced. If the degree of contribution is small or if the crust itself has a rather primitive composition crustal assimilation may not be readily apparent for the Sr-isotopic composition. Given the lack of large differences in element concentration between mantle and crust, reservoir contrasts are expected to be still lower for Nd.

With respect to their Nd isotopic composition the Jurassic arc rocks are depleted (Fig. 5). Therefore, a dominant role of an enriched mantle component during the Jurassic is not very likely. Thus, the Pb isotope composition of the Jurassic lavas, which experienced some degree of crustal contamination or input of subducted sedimentary material, should carry a crustal fingerprint rather than respond subcontinental mantle.

Fig. 5b compares the initial Pb isotopic composition of the Jurassic rocks investigated in this study with those of intrusive and extrusive rocks from the Cretaceous and Miocene to Recent arc systems (data from Haschke et al., 2001; Trumbull et al., 1999). As can be seen from this figure these data define broadly a linear trend. Rocks from the Cretaceous and Miocene to Recent arc extend to higher Pb isotope ratios compared to the Jurassic lavas. We argue that the linear trend defined by all data points mainly represents the crustal Pb growth of the Central Andean crust. The Th/U ratio (3.5–3.8) of the crustal source did not change significantly over time, i.e., there was no involvement of rocks that had higher (>4) or lower (<3.5) Th/U ratios for considerable time. If during the younger arc periods a different basement with distinctive Pb isotopic signatures had been present, it should have fingerprinted the lavas as known from volcanic rocks farther to the north (e.g., Davidson et al., 1990; Wörner et al., 1992). The fact that this is not the case leads us to postulate that the Andean arc segment south of 18°30′S formed on the same type of Palaeozoic basement at least since the Jurassic.

Fig. 5. εNd_i vs. $^{87}Sr/^{86}Sr_i$ and $^{208}Pb/^{204}Pb_i$ vs. $^{206}Pb/^{204}Pb_i$ diagrams for samples from the Jurassic, Cretaceous and Miocene to recent arc systems of the Central Andes. "Mantle array" according to DePaolo and Wasserburg (1979); BSE—Bulk Silikate Earth (upper panel). The lower panel shows lead evolution lines according to the two-stage growth model (Stacey and Kramers, 1975) and the orogen trend according to Plumbotectonics (Zartman and Doe, 1981). Data sources: Jurassic (this study), Cretaceous (Haschke et al., 2001), Miocene to recent (Trumbull et al., 1999).

As seen from the Sr and Nd isotope composition and from trace element data (Fig. 5), the degree of crustal assimilation has increased in the Cretaceous and particular in the modern arc magmas. Influence of extensive amounts of crust is particularly required to account for the crustal-like Sr and Nd isotope ratios of the modern arc lavas. It is generally believed that the modern arc lavas largely carry the trace-element and isotopic characteristics of the continental crust through which they passed. This contamination was aided by a thickened crust of at least 50 km (Trumbull et al., 1999). An estimate of the present-day Nd composition of the Andean crust comes from large-volume siliceous ignimbrites, which are interpreted as nearly pure crustal melts (Francis et al., 1989; Lindsay et al., 2001). These rocks show εNd_i-values between −7 and −10 and $^{87}Sr/^{86}Sr_i$ ratios between 0.709 and 0.713. Among the various Andean volcanic arcs, the Jurassic arc shows the least degree of crustal involvement, and hence, most closely reflects the Sr and Nd isotopic signature of the mantle source. The Pb isotopic signature of the Jurassic arc, however, appears to be largely controlled by crustal contributions.

5.2. Constraints on magma source and evolution

All rocks from the Jurassic arc of the Central Andes in N-Chile investigated in this paper have mantle signatures or contain a substantial mantle component. This is well established as they mostly fall in or around the mantle array in the εNd_i vs. $^{87}Sr/^{86}Sr_i$-diagram (Fig. 5a). This holds true even for the intermediate group IV rocks (Oxfordian) with high SiO_2, and low Cr, Ni, and Mg. Samples K28 and K29 (group III-1) display rather high εNd_i-values of about 5.5 and enhanced $^{87}Sr/^{86}Sr_i$ ratios of up to 0.7056 (Fig. 5a, inset). A similar discrepancy between Nd and Sr isotope ratios was reported from the Samail ophiolite (McCulloch et al., 1980) and the high Sr isotope ratio was explained by interaction with sea water. It is well known that the Rb–Sr isotopic system is sensitive to hydrothermal interactions while the Sm–Nd system appears essentially undisturbed (McCulloch et al., 1980; Michard et al., 1983). Other volcanic rocks of groups II and III also show a slight tendency towards higher Sr isotope ratios, which could likewise be explained by sea water alteration. This is in good agreement with the marine environment of these volcanic series. In contrast, the amphibole-bearing volcanic rocks that extruded subaerial (groups I and IV) do not show higher $^{87}Sr/^{86}Sr_i$ (Fig. 5a). With $^{87}Sr/^{86}Sr_i$ ratios of 0.7040, they indicate only minor or no crustal contribution.

Mantle provenance has also been reported for volcanic rocks of the Jurassic La Negra Formation, dated at 186 and 180 Ma by the K–Ar method (Rogers and Hawkesworth, 1989; Lucassen and Franz, 1994; Pichowiak, 1994) to the south of the study area. In the Th/Yb vs. Ta/Yb-diagram (Fig. 6) basaltic to basaltic andesitic rocks of the Caleta Ligate Formation (group II) and samples K28 and K29 from group III are the only rocks that display a depleted mantle signature. The alkaline basalts from the Cerro Jaspe area (Precordillera; group V) fall into the (asthenospheric) enriched mantle field. These volcanic rocks show the most primitive isotopic composition. Rocks from all other groups have calc-alkaline characteristics.

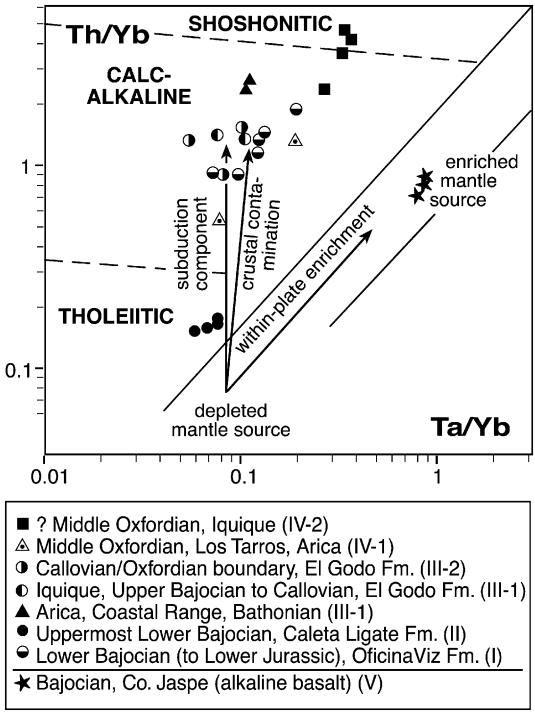

Fig. 6. Th/Yb vs. Ta/Yb-diagram of Jurassic volcanic rocks according to Pearce (1983). The investigated samples display three distinct groups: tholeiitic volcanic rocks with affinity to a depleted mantle source, alkalibasalts with enriched mantle source signatures and basaltic andesites to andesites influenced by subduction or crustal contamination.

The volcanic rocks of the *Oficina Viz Formation (group I)* are thought to have evolved and have been derived from differentiated magmas as indicated by medium to high Mg# values (43–64; Table 2). Their broad band of subparallel curves of immobile REE (Fig. 2) and the large ranges in Ti, Zr, Cr and Ni concentrations (Fig. 3, Table 2) might suggest that most of these rocks belong to a sequence related by fractional crystallization. The large compositional variation implies that pyroxenes, amphiboles, and, to a lesser extent, oxides were important fractionating phases, which agrees with the abundant occurrence of rocks with variable contents (up to 8%) of tschermakitic to pargasitic amphibole phenocrysts (Kramer and Seifert, 2000). Such amphiboles typically crystallize at lower crustal levels in high-Al basaltic systems with up to 5% water content (Foden and Green, 1992).

However, according to Allègre and Minster (1978) and Gill (1981) volcanic rock sequences in log(compatible element)−log(incompatible element) diagrams show convex-down parabola and they define straight lines within linear diagrams in the case of mixing and those distributions seem to be indicated for the Oficina Viz Formation (see trend 1 in the Cr–Zr diagrams, Figs. 3a and d). Therefore, there must

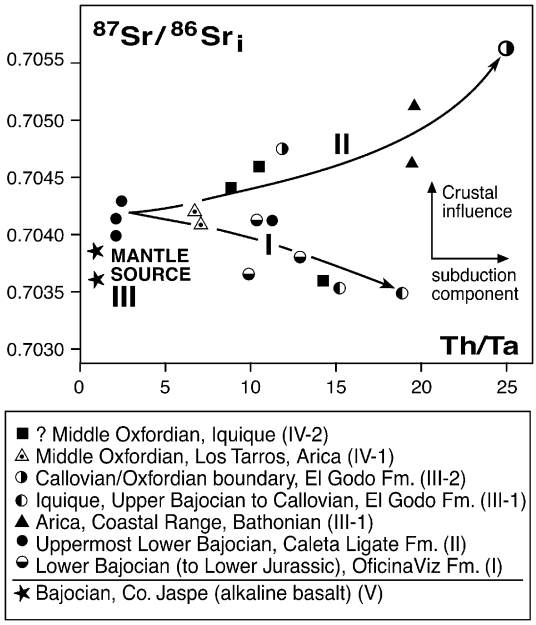

Fig. 7. $^{87}Sr/^{86}Sr$ vs. Th/Ta-diagram of Jurassic volcanic rocks to distinguish crustal contamination and subduction influence by fluid transport on the mantle derived melts. The arrows indicate possible subduction influence (I) or combined subduction and/or crustal influence (II). (III) volcanic rocks with tholeiitic tendency and OIB-type basalts.

have been mixing processes involved in the formation of those rocks. Considering the low $^{87}Sr/^{86}Sr_i$ of these rocks, mixing of different mantle melts seems most likely.

High Ba, Th, and LREE contents in Oficina Viz rocks (Fig. 6, Table 2) reflect possible contributions of subducted material. These elements are preferentially transported by fluids from the slab into the asthenospheric mantle wedge where they can be incorporated into the partial melts (Pearce and Peate, 1995; Tatsumi and Eggins, 1995; Davidson, 1996). Those "subduction components" become more evident if they correlate with low-$^{87}Sr/^{86}Sr_i$ ratio as shown for samples of groups I and III in a $^{87}Sr/^{86}Sr_i$ vs. Th/Ta diagram (Fig. 7).

Caleta Ligate (group II) volcanic rocks define a narrow refractory-element pattern (Fig. 2). These rocks have invariable Mg#-figures at 55, low refractory LILE (Th = 0.29–0.37 ppm), LREE (La/Sm = 0.88–1.9), HFSE (Ta = 0.11–0.22 ppm), and high εNd_i values (4.8–6.4; Fig. 5a). The depleted tholeiitic character suggests that the melts may have been derived from depleted parts of the melting column within the mantle wedge (cf. Pearce and Peate, 1995). Notwithstanding this refractory incompatible element signature, the Caleta Ligate volcanic rocks classify as trachybasalt or basaltic trachyandesite in the TAS diagram according to Le Maitre et al. (1989). This is caused by their higher Na contents, which are predominantly concentrated in plagioclase phenocrysts and groundmass albite. The accumulation of

Na might be due to mantle metasomatism in the wedge as discussed for East-Kamchatka by Kepezhinskas et al. (1995).

The heterogeneous *El Godo Formation (group III)* includes predominantly enriched calc-alkaline basalts to basaltic andesites, and tholeiitic basaltic andesites (K28 and K29). The tholeiitic rocks contain no more than 0.1–0.3 wt% K_2O, 0.1 ppm Ta, 50 ppm Zr, 1.4 ppm Hf, 55 ppm REE, 12 ppm Rb, and 20 ppm Ba. For comparison, the samples K78 and K79 of this group have higher contents of these elements, e.g., up to 330 ppm Ba, 10 ppm Th, 0.5 ppm Ta, and 137 ppm REE. The depleted tholeiitic rocks represent the most primitive (Mg# = 69), the other basaltic andesites the most evolved rocks of group III (Mg# from 36 to 53). Both normal and depleted basaltic andesites display a well-developed negative Nb–Ta anomaly (Fig. 2). High Na (K28 and 29) and enhanced Ba and Th in the other rocks may indicate a subduction component. On the other hand, enrichment of LILE (Th, La) and HFSE (Ta) as well as a moderate decrease of εNd_i from 5.9 to 2.2 in group III basaltic andesites from the coast south of Arica (samples 244 and 245; Tables 2 and 3) is consistent with participation of a crustal component from the overriding upper plate (Hildreth and Moorbath, 1988). The initial Pb isotope compositions of three out of five samples, however, are remarkably unradiogenic. Since these samples are characterized by high Th and U concentrations, and thus have developed rather radiogenic present-day Pb isotope compositions (Table 3), it is unclear whether this signature is real or originates from an overestimation of in situ lead growth.

The Jurassic volcanism in the Arica area terminated during the Middle Oxfordian after the eruption of *intermediate to acid lavas (group IV)*. Tschermakitic and pargasitic amphibole fractionated from those melts as in some of the Oficina Viz volcanic rocks (group I). Group IV-2 rocks from Iquique are strongly altered by oxidation and weathering, which may have affected alkali and other mobile elements like Mg, Ca, and Sr. However, they show lower concentrations of immobile elements such as Y, Yb, and HFSE (Nb, Ta, and Ti). The rocks of group IV plot in the mantle array (Fig. 5a) and have εNd_i as low as 3.5 and 4.1.

Some of the *amphibole-bearing intermediate group I rocks* (V15, V21, La2) and *andesitic to dacitic rocks of group IV* meet the criteria for adakitic rocks ($SiO_2 \geqslant 56\%$, $Al_2O_3 \geqslant 15\%$, MgO mostly <3, rarely >6, high Na_2O ($>5\%$, the most of it incorporated in plagioclase and amphibole), $Sr \geqslant 400$ppm, $Sr/Yb > 40$, generally MORB-like isotope ratios, i.e., $^{87}Sr/^{86}Sr_i < 0.7040$, $Y \leqslant 18$ and $Y \leqslant 1.9$, see Tables 2 and 3) according to Defant and Drummond (1990). However, they have La/Yb = 8–12 and do not reach $La/Yb \geqslant 20$, which was considered to be characteristic of adakites (cf. Defant et al., 1991). Missing positive Sr-anomalies for some Oxfordian adakite-like rocks (Fig. 8) may be due to loss of Sr during the alteration mentioned above.

The adakite composition (Defant et al., 1991) is consistent with partial melting of (garnet) amphibolite to eclogite source rocks, which may derive from subducted oceanic basalt in the slab (cf. the experimental result and data collection by Rapp et al. (1991), Fig. 8). The garnet- and amphibole-rich restites of melting will be depleted in Al and enriched in Y and HREE. Slab melting may occur between about 80–90 km depth, i.e., within the transition area from amphibolite to eclogite facies

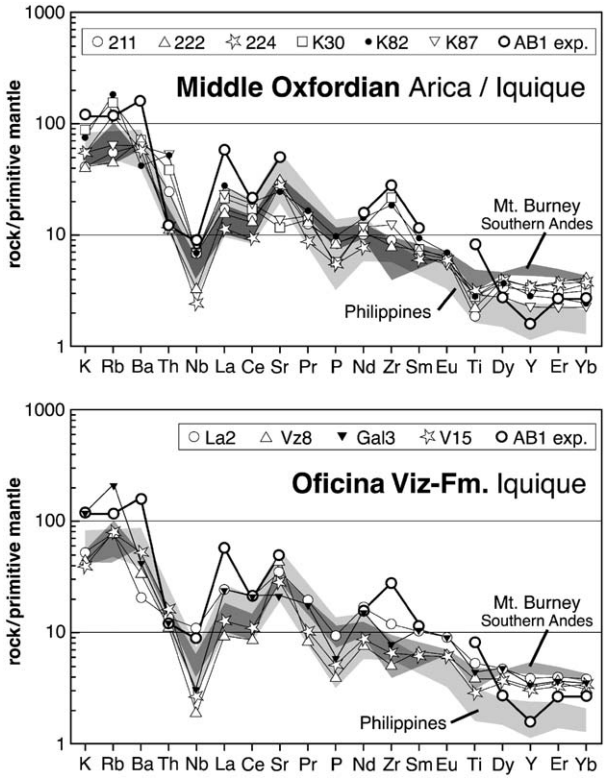

Fig. 8. Extended normalized incompatible element pattern with normalization according to Hofmann (1988) of Oxfordian and Oficina Viz adakite-like andesites and dacites compared with volcanic series of the Philippines (Sajona et al., 1994), Mt. Burney volcanic rocks, Southern Andes according to Stern and Kilian (1996) and an experimental adakitic melt, large circles AB1 (Rapp et al., 1999). Light gray: Philippine adakites, middle grey: Mt. Burney volcanic rocks.

(see Defant and Drummond, 1990; Morris, 1995; Kepezhinskas et al., 1995; Stern and Kilian, 1996).

A comparison of groups I and IV rocks with adakites from Mt. Burney, Southern Andes (Stern and Kilian, 1996) in the incompatible element spider diagrams (Fig. 8) and in a Mg# vs. SiO_2 diagram (Fig. 9) shows a strong overlap with our samples. However, adakites from the Philippine arc (Sajona et al., 1994) and experimental partial melts (Rapp et al., 1999) display more depleted HREE pattern. According to Rapp et al. (1999), interactions between slab melts and peridotite in the mantle wedge may explain adakite-like products enriched in Mg, Cr and Ni like samples V21 and La2 (group I).

An Nb "excess" of the adakitic rocks (Fig. 10a and b) compared with other calc-alkaline basaltic to andesitic rocks (Fig. 10c) from North Chile also emphasize the contribution of slab-melt. Similar adakite-like Quaternary lavas with Nb anomalies

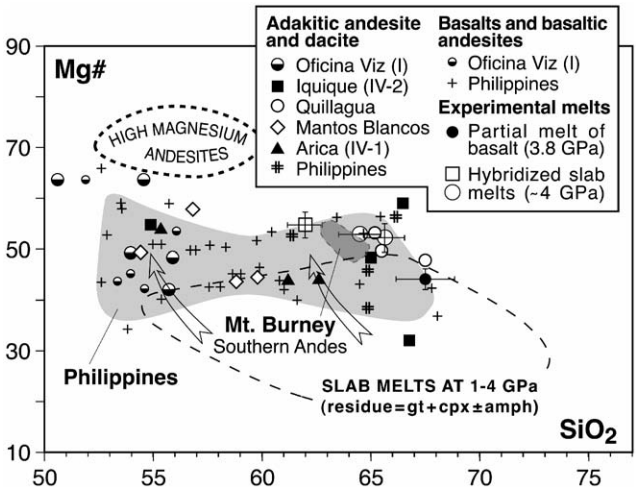

Fig. 9. Comparison of North-Chilean volcanic rocks with experimental melts and Philippine volcanic rocks according to Rapp et al. (1999) in a Mg# vs. SiO_2 diagram (Mg# = 100 Mg/(Mg + Fe_{tot}). SiO_2 concentrations are $H_2O + CO_2$-free calculated. As shown by the filled circle (experimental adakitic melt) vs. great open circles (hybridized slab melts), the melts hybridized due to reaction with peridotite in the mantle wedge thereby shift to higher Mg# (arrows).

(see Fig. 10) and intermediate characteristic between adakite and mantle derived melts from the Ecuadorian Antisana volcano were reported by Bourdon et al. (2002). Those slab melts may have been down-dredged and mixed with mantle melts in the deeper mantle wedge as shown by Bourdon et al. (2003).

Finally, regarding the above comparisons, we find that the Jurassic North Chilean adakite-like rocks only in part are congruent with adakites from other occurrences. Further more, different mixing products of slab and mantle melts occur that do not display all chemical features typical of adakite according to Defant et al. (1991). Nevertheless, it is suggested that those rocks contain a slab component (cf. Bourdon et al., 2002).

The alkaline basalts of *Cerro Jaspe (group V)* form a homogeneous group that is characterized by Mg# = 54, nearly identical incompatible element patterns with positive Nb–Ta–Ti anomalies (Fig. 2, V), uniform ratios of Th/Ta = 1.0, Ta/Yb = 0.81, and La/Sm = 2.42, and TiO_2 varies between 3.6 and 4.1 wt% which fall in the range of ocean island basalt (OIB) type (Sun and McDonough, 1989). These geochemical signatures do not seem to have been affected by the variable degree of carbonatization and chloritization seen in these rocks. Compatible element contents of Cr, Ni, and Sc are also nearly invariable at 220, 83, and 23 ppm, respectively (Fig. 3a, c and d for Cr and Y). This element invariability indicates that the melts from which the alkaline volcanic rocks are directly derived, did not experience a considerable internal differentiation. However, their comparatively low Mg# = 54 (65 is typical of alkaline basalt) and Ni concentrations = 80 ppm (> 200 is typical of

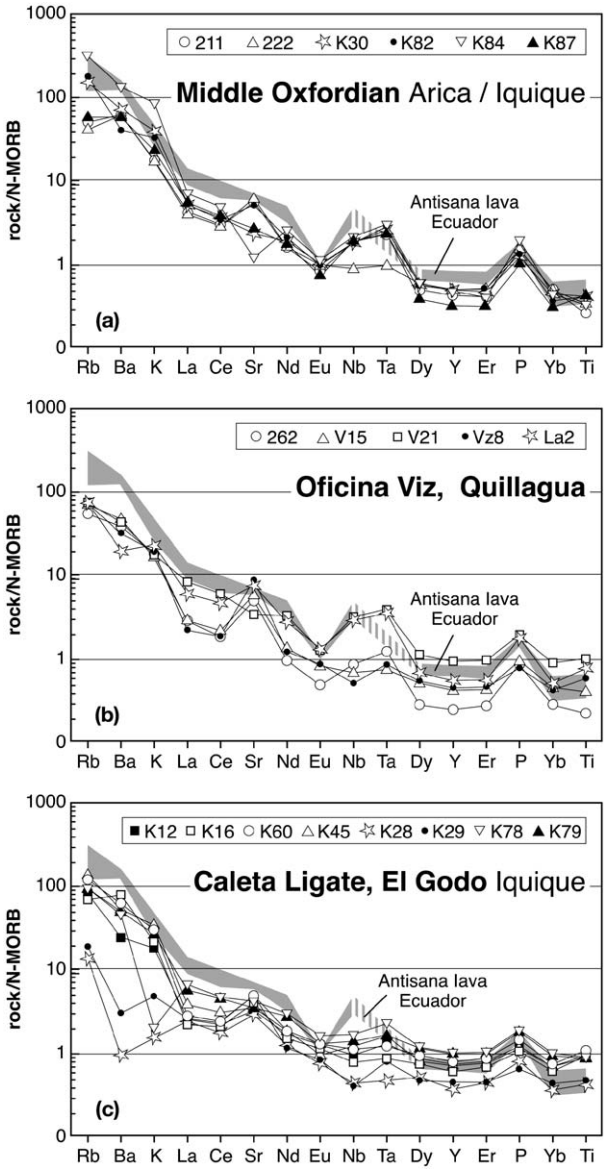

Fig. 10. Positive Nb anomalies within extended trace-element plots normalized to N-MORB according to Sun and McDonough (1989). A comparison of Ecuadorian Antisana lava (according to Bourdon et al., 2002) with basaltic to andesitic/dacitic Jurassic volcanic rocks of North-Chile. Niobium is supposed to be immobile in aqueous solutions (Keppler, 1996; Tatsumi and Kogiso, 1997). However, within the MORB-normalized plot of incompatible elements—arranged according to the degree of enrichment expected in slab fluids from right to left (according to Maury et al., 1992)—Nb appears as positive anomaly. This is consistent with a transport of Nb in slab melt as a metasomatic agent rather than by aqueous solutions from the slab (Bourdon et al., 2002).

alkaline basalt) probably result from strong olivine fractionation of a mantle melt that was derived from an enriched mantle (OIB) source (Fig. 6).

Except for the mobile Cs, their element patterns do not show anomalies that might indicate contributions from a down-going slab or an LILE enriched mantle wedge (Fig. 2,V).

5.3. Tectonic implications

Scheuber and Reutter (1992) apply a tectonic model with a subduction obliqueness of 45° to >90° to the Jurassic magmatic arc between 21° and 25°S, where "strong strike-slip movements and orogen-normal extension operated simultaneously". The extrusion of the Jurassic volcanic deposits of the Oficina Viz-, Caleta Ligate- and El Godo-Formations (18°30′ and 20°30′S) with a probable onset during Sinemurian, falls into episodes of strike-slip tectonics.

During the early period of the oblique subduction with a high rate of subduction shear heating (Peacock, 1996) the mantle immediately above the down-going oceanic plate has not yet cooled down (Defant and Kepezhinskas, 2001). During this stage P–T conditions might have existed which enabled the production of slab melts. This may have been the case during Sinemurian to earlier Bajocian in the initiation stage of the Jurassic subduction, when the lavas of the Oficina Viz Formation with adakitic compositions were produced.

The strike-slip fault system of the upper crust combined with feeder dykes in the deeper lithosphere (cf. Grocott et al., 1994) locally and at times facilitated a fast uprise of minor evolved tholeiitic melt like those of the group III-1 from the asthenospheric mantle. Other uprising mafic magmas evolved within near MOHO lower crustal (tschermakitic ampibole crystallization) and upper crustal (growth of zonal plagioclase) magma chambers.

Basalts and basaltic andesites occur in two coast-parallel belts of different age. The older volcanic zone (Officina Viz Formation, earlier Bajocian to possibly Lower Jurassic) spreads over the inner Coastal Cordillera. The younger Middle Jurassic Caleta Ligate Formation (group II), and El Godo Formation as well as its equivalents in the Arica region (group III) are situated on a broad front at the modern coast line and, indicated by pyroclastic and volcaniclastic products and gravimetrical results extend seawards to the west from it. Since the early Middle Jurassic, the back-arc sea transgressed from the east to the western Coastal Cordillera, which is proofed biostratigraphically (Kossler, 1998). Thus, the eastern margin of the Middle Jurassic volcanic zone is considered as the transition to the western rim of the back-arc in the east (see Fig. 1).

Both the tholeiitic Caleta Ligate basalts of the Coastal Cordillera (group II) and the alkaline Cerro Jaspe basalts, group V (Precordillera) extruded at about 170 Ma. The alkaline basalts of the Cerro Jaspe either show that the Jurassic transtensional tectonic system may have been accompanied by deep-seated magmatism from the asthenospheric mantle also in the easternmost back-arc or—more likely—that this alkaline volcanism indicates a continental rift structure to the east of the arc.

According to Grocott et al. (1994) and Dallmeyer et al. (1996), which dated the plutonism in the area between Taltal and Copiapo, Scheuber and Gonzalez (1999) confirmed a stage of arc-normal extension with the emplacement of large calc-alkaline plutons from 160 to 150 Ma for the area south of Tocopilla. During that time span, at ca. 155 Ma, the eruption of the Oxfordian amphibol-bearing andesites and dacites (group IV) took place. Scheuber and Gonzalez (1999) explain this change in extensional regime within the upper plate by a change from a high- to a low-stress subduction, which "implies a fast foundering of the subducting plate and thus an increased rollback rate of the trench" together with uncoupling of upper and down-going plates. According to Martin (1999), shear stress can also assist slab melting in the case of high subduction rates, which might be the background for generating slab melt component of group IV volcanic rocks.

6. Conclusions

The Jurassic evolution of the Coastal Cordillera in the Iquique–Arica section, N-Chile, comprises a long-lasting (from $\geqslant$175 to $\leqslant$155 Ma) subduction-related calc-alkaline, tholeiitic, and minor alkaline volcanic activity.

Isotopic composition and minor and trace element signature of the lavas reflect magma evolution by fractional crystallization, melt-peridotite reaction, minor crustal assimilation and mixing of predominantly mantle- and slab-derived melts and metasomatic fluid components. The following criteria confirm an active continental margin setting of the investigated segment of the Jurassic Andean volcanic arc: their Pb isotopic composition, which is influenced by a Paleozoic basement, a large share of about 20% of silica-rich dacitic to rhyolitic rocks as well as the higher contents in Ba, Zr, and Th (Gill, 1981) compared with island arc mafic volcanic rocks.

The geochemical and genetic character of the volcanic associations of the Jurassic arc closely correspond with its tectonic evolution inferred from sedimentological-paleogeographic results, and from the fault systems in the lithosphere.

During the first stage of volcanism basaltic-andesitic to adakite-like rocks (group I) were formed from mantle wedge and slab components in the inner Coastal Cordillera. Group IV Oxfordian volcanism show predominantly adakitic features and correlate with extensional tectonics and increased subduction rate. They may include portions of slab melts that terminate the Upper Jurassic arc volcanism in the Iquique–Arica area. Both formations with slab-component are characterized by a higher Nb content than expected in the case of transport by slab fluids, high Sr/Y ratio and low-HREE contents. During the Middle Jurassic tholeiitic and calc-alkaline weakly and stronger evolved basalts and basaltic andesites have been transported and stored within the system of deep-seated feeder fissures and strike-slip faults and erupted in the volcanic arc in the present-day western Coastal Cordillera. A continental alkaline basaltic volcanism with OIB signatures in the Cerro Jaspe area (Precordillera) approximately 70 km to the east of the arc/back-arc

boundary, marks the area without subduction influence on the volcanism during the Middle Jurassic.

The $^{87}Sr/^{86}Sr_i$ and εNd_i ratios mostly fall in the depleted mantle range although some crustal component may be involved. The Pb isotopic composition of the arc rocks is decoupled from the isotopic composition of Sr and Nd. Because the Pb isotopic composition in arc systems is dominated by the crustal component and the Cretaceous and Modern arc volcanic rocks show Pb isotopic compositions that can be largely explained by in situ Pb isotope growth since the Jurassic we argue that the different Andean arc systems between 19/20° to 22°S formed on the same basement type.

The trenchward shift of the volcanic zone during Middle Jurassic on a broad front between 19°30′ and 21°S, the westward movement of magma sources, and of the arc/back-arc boundary combined with a westward arc migration beyond the current coast line agree with a rollback of subduction discussed by Scheuber and Gonzalez (1999). From the temporal distribution of the Jurassic volcanic arc lavas on land and its indications at the coast line and westwards, we assume a strong subduction erosion of the Jurassic magmatic arc particularly in its northern part. In the context with the renewed migration of the magmatic activities to the east (plutonism of the Late Jurassic and Early Cretaceous volcanism) we would like to describe the study area as oscillating arc section.

Acknowledgement

W.K. would like to thank A.V. Hillebrandt, A. Kossler, H.-G. Wilke, and S. Wittmann for joint field work, helpful information and discussions. We thank G. Wörner, G.L. Farmer, and K. Heide for their comments, which improved the manuscript considerably.

This contribution is part of the German Collaborative Research Center SFB 267 ''Deformation processes in the Andes'' supported by the German Research Council (DFG).

References

Allègre, C.J., Minster, J.F., 1978. Quantitative models of trace element behavior in magmatic processes. Earth Planet. Sci. Lett. 38, 1–25.

Bourdon, E., Eissen, J.-P., Monzier, M., Robin, C., Martin, H., Cotton, J., Hall, M.L., 2002. Adakite-like lavas from Antisana volcano (Ecuador): evidence for slab melt metasomatism beneath the Andean Northern Volcanic Zone. J. Petrol. 43, 199–217.

Bourdon, E., Eissen, J.-P., Gutscher, M.-A., Monzier, M., Hall, M.L., Cotton, J., 2003. Magmatic response to early aseismic ridge subduction: the Ecuadorian margin case (South America). Earth Planet. Sci. Lett. 205, 123–138.

Buchelt, M., Tellez, C., 1988. The Jurassic La Negra Formation in the area of Antofagasta, Northern Chile (lithology, petrography, geochemistry). In: Bahlburg, H., Breitkreuz, C., Giese, P. (Eds.), The Southern Central Andes Lecture Notes on Earth Sciences, Vol. 17. Springer, Berlin, pp. 171–182.

Buchelt, M., Zeil, K., 1986. Petrographische und geochemische Untersuchungen an jurassischen Vulkaniten der Porphyrit-Formation in der Küstenkordillere Nord-Chiles. Berl. Geowiss. Abh. (A) 66, 191–204.

Coira, B., Davidson, J., Mpodozis, C., Ramos, V., 1982. Tectonic and magmatic evolution of the Andes of northern Argentina and Chile. Earth Sci. Rev. 18, 253–283.

Dallmeyer, R.D., Brown, M., Grocott, J., Taylor, G.K., Treloar, P.J., 1996. Mesozoic magmatic and tectonic events within the Andean plate boundary zone, 26°–27°30′S, North Chile: constraints from $^{40}Ar/^{39}Ar$ mineral ages. J. Geol. 104, 19–40.

Davidson, J.P., 1996. Deciphering mantle and crustal signatures in subduction zone magmatism. In: Bebout, G.E., Scholl, D.W., Kirby, S.H., Platt, J.P. (Eds.), Subduction: Top to bottom, Geophysical Monograph. Vol. 96, pp. 251–262.

Davidson, J., Godoy, E., Covacevich, V., 1976. El Bajociano marino de Sierra Minillas (70°39′L.O-26°L.S) y Sierra Fraga (69°50′L.O–27°L.S), Provincia de Atacama, Chile; edad y marco geotectónico de la Formación La Negra en esta latitud. Congr. Geol. Chil. Actas. 1, A255–A272.

Davidson, J., McMillan, N., Moorbath, S., Wörner, G., Harmon, R., Lopez-Escobar, L., 1990. The Nevados de Payachata volcanic region (18°S/69°W, N. Chile) II. Evidence for widespread crustal involvement in Andean magmatism. Contrib. Miner. Petrol. 105, 412–432.

Defant, M.J., Drummond, M.S., 1990. Derivation of some modern arc magmas by melting of young subducted lithosphere. Nature 347, 662–665.

Defant, M.J., Kepezhinskas, P., 2001. Evidence suggests slab melting in arc magmas. EOS Trans. Am. Geophys. Union 82, 65–69.

Defant, M.J., Clark, L.F., Steward, R.H., Drummond, M.S., de Boer, J.Z., Maury, R.C., Bellon, H., Jackson, T.E., Restrepo, J.F., 1991. Andesite and dacite genesis via contrasting processes: the geology and geochemistry of El Valle Volcano, Panama. Contrib. Mineral. Petrol. 106, 309–324.

DePaolo, D.J., Wasserburg, G.J., 1979. Petrogenetic mixing models and Nd–Sr isotopic pattern. Geochim. Cosmochim. Acta 43, 615–627.

Foden, J.D., Green, D.H., 1992. Possible role of amphibole in the origin of andesite: some experimental and natural evidence. Contrib. Mineral. Petrol. 109, 479–493.

Francis, P.W., Sparks, R.S.J., Hawkesworth, C.J., Thorpe, R.S., Pyle, D.M., Tait, S.R., Mantovani, M.S., McDermott, F., 1989. Petrology and geochemistry of volcanic rocks of the Cerro Galán caldera, northwest Argentina. Geol. Mag. 126, 515–547.

Gill, J.B., 1981. Orogenic andesites and plate tectonics. Springer, Berlin, Heidelberg, New York pp. 1–390.

Grocott, J., Brown, M., Dallmeyer, R.D., Taylor, G.K., Treloar, P.J., 1994. Mechanisms of continental growth in extensional arcs: an example from the Andean plate-boundary zone. Geology 22, 391–394.

Gröschke, M., Wilke, H.-G., 1986. Lithology and stratigraphy of Jurassic sediments in the North Chilean Pre-Cordillera between 21°30′ and 22°S. Zbl. Geol. Paläont. Teil. 1, 1317–1324.

Haschke, M., Siebel, W., Günther, A., Scheuber, E., 2001. Repeated crustal thickening and recycling during the Andean orogeny in North Chile (21–26°S). J. Geophys. Res. 106, 1–18.

Hildreth, W., Moorbath, S., 1988. Crustal contributions to arc magmatism in the Andes of Central Chile. Contrib. Mineral. Petrol. 98, 455–489.

Hofmann, A.W., 1988. Chemical differentiation of the earth: the relationship between mantle, continental crust and oceanic crust. Earth Planet. Sci. Lett. 90, 243–262.

Jaillard, E., Soler, P., Carlier, G., Mourier, T., 1990. Geodynamic evolution of the northern and central Andes during early to middle Mesozoic times: a Tethyan model. J. Geol. Soc. Lond. 147, 1009–1022.

Kepezhinskas, P.K., Defant, M.J., Drummond, M.S., 1995. Na metasomatism in the island-arc mantle by slab melt-peridotite interaction: evidence from mantle xenoliths in the North Kamchatka arc. J. Petrol. 36, 1505–1527.

Keppler, H., 1996. Experimental constraints on trace element transport by fluids in subduction zones. EOS Trans. Am. Geophys. Union, Fall Meeting Suppl., 655 (abstract)

Kossler, A., 1998. Der Jura in der Küstenkordillere von Iquique (Nordchile)- Paläontologie, Lithologie, Stratigraphie, Paläogeographie. Berliner Geowiss. Abh. (A) 197, Berlin, pp. 1–226

Kösters, M., Götze, H.-J., Schmidt, S., Fritsch, J., Araneda, M., 1997. Gravity field of a continent-ocean transition mapped from land, air, and sea. EOS 78, 13–16.

Kramer, W., Seifert, W., 2000. Adakites within the Jurassic volcanic arc of the Coastal Cordillera, N-Chile. AGU Fall Meeting 2000, San Francisco. EOS Trans. Am. Geophys. Union 81, F1316 (abstract)

Le Maitre, R.W., Bateman, P., Dudek, A., Keller, J., Lameyre Le Bas, M.J., Sabine, P.A., Schmid, R., Sørensen, H., Streckeisen, A., Woolley, A.R., Zanettin, B., 1989. A Classification of Igneous Rocks and Glossary of Terms. Blackwell Scientific Publications, Oxford pp. 1–193.

Lindsay, J.M., Schmitt, A.K., Trumbull, R.B., De Silva, S.L., Siebel, W., Emmermann, R., 2001. Magmatic evolution of the La Pacana Caldera System, Central Andes, Chile: compositional variation of two cogenetic, large-volume felsic ignimbrites. J. Petrol 42, 459–486.

Lucassen, F., Franz, G., 1994. Arc related Jurassic igneous and meta-igneous rocks in the Coastal Cordillera of northern Chile/Region Antofagasta. Lithos 32, 273–298.

Lucassen, F., Fowler, C.M.R., Franz, G., 1996. Formation of magmatic crust at the Andean continental margin during early Mesozoic: a geological and thermal model of the North Chilean Coast Range. Tectonophysics 262, 263–279.

MacLean, W.H., Barret, T.J., 1993. Lithochemical techniques using immobile elements. J. Geochem. Explor. 48, 109–133.

Manhès, G., Minster, J.F., Allègre, C.J., 1978. Comparative uranium–thorium–lead and rubidium–strontium study of the Saint-Séverin amphoterite: consequences for early solar system chronology. Earth Planet. Sci. Lett. 39, 14–24.

Martin, H., 1999. Adakitic magmas: modern analogues of Archaean granitoids. Lithos 46, 411–429.

Maury, R.C., Defant, M.J., Joron, J.-L., 1992. Metasomatism of the sub-arc mantle inferred from trace elements in Philippine xenoliths. Nature 360, 661–663.

McCulloch, M.T., Gregory, R.T., Wasserburg, G.J., Taylor Jr., H.P., 1980. A Neodymium, Strontium, and Oxygen isotopic study of the Cretaceous Samail Ophiolite and implications for the petrogenesis and seawater-hydrothermal alteration of oceanic crust. Earth Planet. Sci. Lett. 46, 201–211.

Michard, A., Albarède, F., Michard, G., Minster, J.F., Charlous, J.L., 1983. Rare-earth elements and uranium in high-temperature solutions from East Pacific Rise hydrothermal vent field (13°N). Nature 303, 795–797.

Morris, P.A., 1995. Slab melting as an explanation of Quaternary volcanism and aseismicity in southwest Japan. Geology 23, 395–398.

Mpodozis, C., Ramos, V., 1990. The Andes of Chile and Argentina. In: Ericksen, G.E., Cañas Pinochet, M.T., Reinemund, J.A. (Eds.), Geology of the Andes and its relation to hydrocarbon and mineral resources. Houston, Texas, Circum-Pacific Council for Energy and Mineral Resources. Earth Science Series 11, pp. 59–90.

Palacios, M.C., 1978. The Jurassic Paleovolcanism in Northern Chile. Dissertation, Eberhard-Karls-Universität Tübingen.

Pálfy, J., Smith, P.L., Mortensen, J.K., 2000. A U–Pb and $^{40}Ar/^{39}Ar$ time scale for the Jurassic. Can. J. Earth Sci. 37, 923–944.

Peacock, S.M., 1996. Thermal and petrologic structure of subduction zones. In: Bebout, G.E., Scholl, D.W., Kirby, S.H., Platt, J.P. (Eds.), Subduction: Top to bottom. Geophysical Monograph 96, pp. 119–133.

Pearce, J.A., 1983. Role of the sub-continental lithosphere in magma genesis at active continental margins. In: Hawkesworth, C.J., Norry, M.J. (Eds.), Continental basalts and mantle xenoliths. Shiva, Nentwich, pp. 230–249.

Pearce, J.A., Peate, D.W., 1995. Tectonic implications of the composition of volcanic arc magmas. Ann. Rev. Earth Planet. Sci. 23, 251–285.

Peccerillo, A., Taylor, S.R., 1976. Geochemistry of Eocene calc-alkaline volcanic rocks from the Kastamonu area, northern Turkey. Contrib. Mineral. Petrol. 58, 63–81.

Pelz, K., 2000. Tektonische Erosion am zentralandinen Forearc (20–24°S). Scientific Technical Report STR00/20, Potsdam, pp. 1–118.

Pichowiak, S., 1994. Early Jurassic to Early Cretaceous magmatism in the Coastal Cordillera and the Central Depression of North Chile. In: Reutter, K.J., Scheuber, E., Wigger, P. (Eds.), Tectonics of the Southern Central Andes. Springer, Berlin, pp. 203–217.

Rapp, R.P., Watson, E.B., Miller, C.F., 1991. Partial melting of amphibolite/eclogite and the origin of Archean trondhjemites and tonalites. Precambrian Res. 51, 1–25.

Rapp, R.P., Shimizu, N., Norman, M.D., Applegate, G.S., 1999. Reaction between slab-derived melts and peridotite in the mantle wedge: experimental constraints at 3.8 GPa. Chem. Geol. 160, 335–356.

Rogers, G., Hawkesworth, C.J., 1989. A geochemical traverse across the North Chilean Andes: evidence for crust generation from the mantle wedge. Earth Planet. Sci. Lett. 91, 271–285.

Sajona, F.G., Bellon, H., Maury, R.C., Pubellier, M., Cotton, J., Rangin, C., 1994. Magmatic response to abrupt changes in geodynamic settings: Pliocene-Quaternary calc-alkaline and Nb-enriched lavas from Mindanao (Philippines). Tectonophysics 237, 47–72.

Scheuber, E., Gonzalez, G., 1999. Tectonics of the Jurassic–Early Cretacous magmatic arc of the north Chilean Coastal Cordillera (22°–26°S): a story of crustal deformation along a convergent plate boundary. Tectonics 18, 895–910.

Scheuber, E., Reutter, K.-J., 1992. Magmatic arc tectonics in the Central Andes between 21° and 25°S. Tectonophysics 205, 127–140.
Sempére, T., 1995. Phanerozoic evolution of Bolivia and adjacend regions. In: Tankard, A.J., Suárez Soruco, R., Welsink, H.J. (Eds.), Petroleum Basins of South America. AAPG Memoir 62, pp. 207–230.
Stacey, J.S., Kramers, J.D., 1975. Approximation of terrestrial lead isotope evolution by a two-stage model. Earth Planet. Sci. Lett. 26, 207–221.
Stern, C.R., Kilian, R., 1996. Role of the subducted slab, mantle wedge and continental crust in the generation of adakites from the Andean Austral Volcanic Zone. Contrib. Mineral. Petrol 123, 263–281.
Sun, S.-S., 1980. Lead isotopic study of young volcanic rocks from mid ocean ridges, ocean islands and island arcs. R. Soc. London Philos. Trans. 297, 409–445.
Sun, S.S., McDonough, W.F., 1989. Chemical and isotopic systematics of oceanic basalts: implications for mantle composition and processes. Geol. Soc. Spec. Pub. 42, 313–345.
Tatsumi, Y., Eggins, S., 1995. Subduction Zone Magmatism. Blackwell Science, Oxford pp. 1–211.
Tatsumi, Y., Kogiso, T., 1997. Trace element transport during dehydration processes in the subducted oceanic crust: origin of chemical and physical characteristics in arc magmatism. Earth Planet. Sci. Lett. 148, 207–222.
Thomas, A., 1970. Quadrángulos Iquique y Caleta Molle. Inst. Inv. Geol., Cartas 21/22, Santiago de Chile, pp. 1–52.
Tilton, G.R., 1973. Isotopic lead ages of chondritic meteorites. Earth Planet. Sci. Lett. 19, 321–329.
Trumbull, R.B., Wittenbrink, R., Hahne, K., Emmermann, R., Büsch, W., Gerstenberger, H., Siebel, W., 1999. Evidence for Late Miocene to Recent contamination of arc andesites by crustal melts in the Chilean Andes (25–26°S) and its geodynamic implications. J. South Am. Earth Sci. 12, 135–155.
von Hillebrandt, A., 1996. Der Westrand des Backarc-Beckens im Trias/Jura-Grenzbereich östl. Antofagasta (Nordchile). Terra Nostra (15. Geowiss Lateinamerika Koll.) 8, 65.
von Hillebrandt, A., Kramer, W., Bartsch, V., Bebiolka, A., Kossler, A., Wittmann, S., 1998. Vulkanismus und Sedimentation in Trias und Jura der Küstenkordillere von Nordchile–Beitrag zur Rekonstruktion des jurassischen magmatischen Bogens. In: Deformationsprozesse in den Anden. Sonderforschungsbereich 267, Berlin, Potsdam, Berichtsband 1996–1998, pp. 523–559.
von Huene, R., Weinrebe, W., Heeren, F., 1999. Subduction erosion along the North Chile margin. J. Geodynamics 27, 345–358.
von Hillebrandt, A., Bartsch, V., Bebiolka, A., Kossler, A., Kramer, W., Wilke, H.-G., Wittmann, S., 2000. The paleogeographic evolution in a volcanic-arc/back-arc setting during the Mesozoic in northern Chile. Z. Angew. Geol. SH1 2000, Hannover, pp. 87–93.
Weaver, B.L., Tarney, J., 1980. Rare earth geochemistry of Lewisian granulite-facies gneisses, NW Scottland: implications of the Archaean lower continental crust. Earth Planet. Sci. Lett. 51, 279–296.
Winchester, J.A., Floyd, P.A., 1977. Geochemical discrimination of different magma series and their differentiation products using immobile elements. Chem. Geol. 20, 325–343.
Wittmann, S., 1999. Die fazielle Entwicklung des jurassischen "back arc"-Beckens in der Küstenkordillere von N-Chile zwischen Zapiga und Arica (19°38′/18°28′). Terra Nostra 99/4, 295–296.
Wörner, G., Moorbath, S., Harmon, R.S., 1992. Andean Cenozoic volcanic centres reflect basement isotopic domains. Geology 20, 1103–1106.
Zartman, R.T., Doe, B.R., 1981. Plumbotectonics—The model. Tectonophysics 75, 135–162.
Zindler, A., Hart, S.R., 1986. Chemical geodynamics. Ann. Rev. Earth Planet. Sci. 14, 493–571.
Zuleger, E., Erzinger, J., 1988. Determination of the REE and Y in silicate materials with ICP-AES. Fresenius Z. Anal. Chem. 332, 140–143.